Electronic Supplementary Material (ESI) for Chemical Science.
This journal is © The Royal Society of Chemistry 2021

Supporting Information

For

Rational Design of a Photoswitchable DNA Glue Enabling High Regulatory Function and Supramolecular Chirality Transfer

Nadja A. Simeth,[a] Shotaro Kobayashi,[b] Piermichele Kobauri,[a] Stefano Crespi,[a] Wiktor Szymanski,[a,c] Kazuhiko Nakatani,[b],* Chikara Dohno,[b],* and Ben L. Feringa[a],*

[a]Centre for Systems Chemistry, Stratingh Institute for Chemistry, Faculty for Science and Engineering, University of Groningen, Nijenborgh 4, 9747 AG Groningen, The Netherlands.
[b]Department of Regulatory Bioorganic Chemistry, The Institute of Scientific and Industrial Research, Osaka University, 8-1 Mihogaoka, Ibaraki 567-0047, Japan.
[c]Department of Radiology, Medical Imaging Center, University of Groningen, University Medical Centre Groningen, Hanzeplein 1, 9713 GZ Groningen, The Netherlands.

Table of Contents

1. Synthesis and Characterization

1.1. General Remarks

Synthesis and isolation of compounds. DNA was purchased from Integrated DNA Technologies, Thermo Fisher Scientific, and Eurofins genomics. All chemicals for synthesis were obtained from commercial sources (Sigma-Aldrich, TCI, Alfa Aesar, and Boom) and used as received unless stated otherwise. Solvents used were reagent grade for synthesis and technical grade for isolation if not otherwise stated. Dry solvents were collected from a Pure Solve MD5 solvent dispenser from Demaco or by drying them for 48 h over fresh 3 Å molecular sieves. For thin-layer chromatography (TLC) aluminum foils with a silica gel matrix (Supelco, silica gel 60, 56524) were used, and components were visualized with a UV lamp at 254 nm or through staining with NH_4CeSO_4 x H_2O (10 g/L) or ninhydrin if necessary. Flash chromatography was performed on a Büchi Reveleris® X2 flash chromatography system on Büchi EcoFlex silica columns (4 - 40 g, 40−63 µM, 60 Å). HPLC purifications were conducted with a JASCO HPLC system consisting of PU-4086 Binary semi-preparative pump and UV-4070 UV-vis detector. Compounds were purified with a reversed phase column (COSMOSIL $5C_{18}$-MS-II, 20ID*150 mm) using a linear gradient (from 5% to 40% for 45 min) of acetonitrile in 0.1% aqueous AcOH at a flow rate of 10 mL/min. The effluent was monitored at 254 nm.

Compound characterization. Nuclear magnetic resonance spectroscopy (NMR) was carried out using an Agilent Technologies 400-MR (400/54 Premium Shielded) spectrometer (400 MHz), JEOL JNM-LA400 (400 MHz), and Bruker BioSpin AVANCEIII700 (700 MHz) and recoded at room temperature (22–24 °C). Chemical shifts are reported in δ[ppm] relative to an internal standard (solvent residual peak). The solvents used are indicated for each spectrum. Coupling constants are reported in Hertz [Hz]. Characterization of the signals: s = singlet, d = doublet, t = triplet, q = quartet, m = multiplet, *b*s = broad singlet, dd = doublet of doublet, dt = doublet of triplet. Integration is directly proportional to the number of the protons. Characterization of the ^{13}C-NMR signals: (+) for CH_3 or CH, (-) for CH_2 and (q) for quaternary C-atoms. The latter assignment resulted from DEPT135. Infrared (IR) spectra were recorded on a PerkinElmer UATR (Single Reflection Diamond) Spectrum Two device (4000−700 cm^{-1}; resolution 4 cm^{-1}). Melting point ranges were determined on a Stuart analogue capillary melting point SMP11 apparatus. High Resolution Mass Spectra were recorded on a Thermofisher LTQ Orbitrap XL with eluent MeOH (0.1% FA) and flow rate of 0.15 mL/min^{-1} in positive (ACPI/ESI) mode. For analytical RP-HPLC, a JASCO HPLC system consisting of PU-2084 Quaternary gradient pump and MD-2010 Multiwavelength detector was used. Compounds were analyzed with a reversed phase column (COSMOSIL $5C_{18}$-MS-II, 4.6ID*150 mm) using a linear gradient (from 0% to 30% for 30 min) of acetonitrile in 0.1% aqueous AcOH at a flow rate of 1 mL/min. The effluent was monitored at 251 nm.

1.2. Synthetic Procedures

Route 1: Alkylation as Key Step

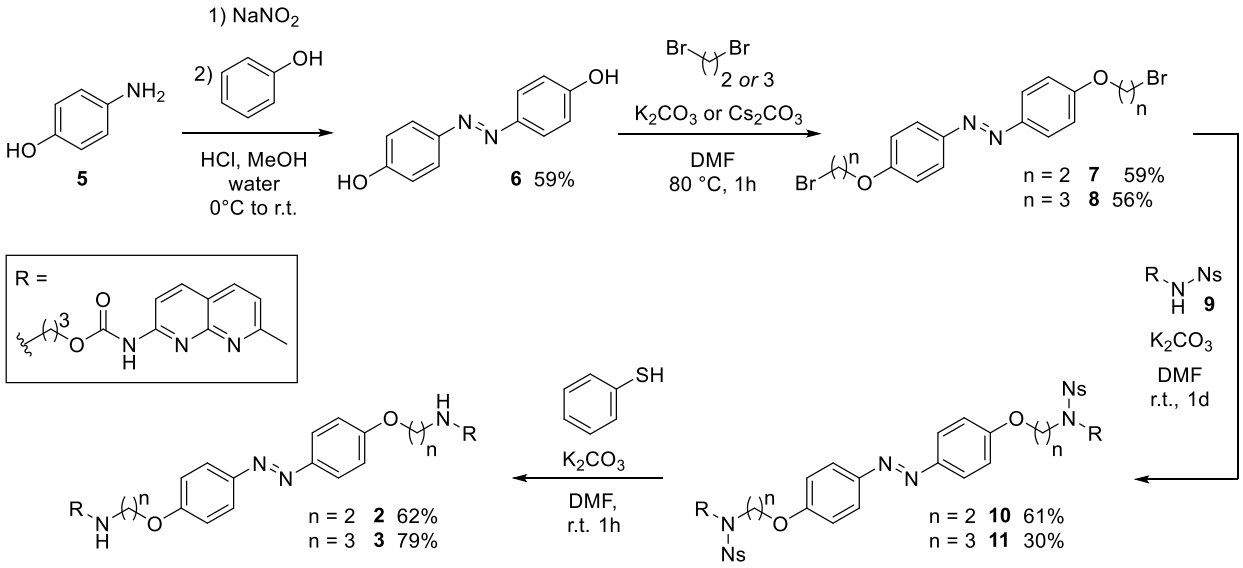

Scheme S1. Synthesis of target compounds **2** and **3** *via N*-alkylation as the key step.

(*E*)-4,4'-(Diazene-1,2-diyl)diphenol (6)[1]

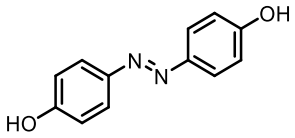

A solution of 4-aminophenol (5.00 g, 45.82 mmol) in HCl (1M, aq, 100 mL) was cooled to 0 °C and $NaNO_2$ (4.67 g, 67.70 mmol) in water (75 mL) was added through a dropping funnel. The reaction mixture was stirred for 1h, diluted with cold MeOH (100 mL) and stirred for an additional 40 min. Then, phenol (4.31 g, 45.80 mmol) in NaOH (3M, aq, 32.5 mL) was added to the reaction mixture at 0 °C through a dropping funnel. Stirring was continued for 30 min at 0 °C and additional 2 h at ambient temperature. The dark solution was acidified with HCl (36% aq.). The formed precipitated was filtered off, washed with water, and dried under vacuum to give the title compound as dark solid (5.79 g, 27.02 mmol, 59%). The compound was converted without further purification. An analytical sample was purified by column chromatography on silica gel (pentane / EtOAc = 1:1) to result in a yellow powder. ^{1}H NMR (400 MHz, Chloroform-*d* : Methanol-*d4* 1:1) δ = 7.73 (d, J = 8.8 Hz, 4H), 6.86 (d, J = 2.1 Hz, 4H). The analytical data was in agreement with published data.[1]

(*E*)-1,2-bis(4-(2-bromoethoxy)phenyl)diazene (7)

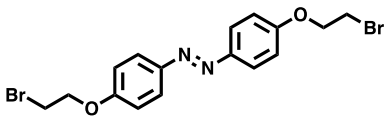

To a solution of anhydrous potassium carbonate (485 mg, 3.51 mmol) in dry acetone (5 mL) was added 4,4'-dihydroxyazobenzene **6** (107 mg, 0.50 mmol) and dibromomethane (1.02 g, 5.43 mmol). The solution was stirred at 70 ºC for 24 h before the reaction mixture was poured

into water. The solution was extracted with EtOAc. The yellow phase was washed with water several times, dried over anhydrous $MaSO_4$ and the solvent was removed under reduced pressure. The residue was purified by column chromatography on silica gel ($CHCl_3$ / MeOH = 10:1) to give **7** (127 mg, 0.30 mmol, 59%) as a yellow powder. ^{1}H NMR ($CDCl_3$, 400 MHz) δ = 7.88 (d, 4H), 7.01 (d, 4H), 4.38 (t, 4H), 3.68 (t, 4H).

(*E*)-3-((N-(2-(4-((4-(2-((N-(3-(((7-methyl-1,8-naphthyridin-2-yl)carbamoyl)oxy)propyl)-2-nitrophenyl)sulfonamido)ethoxy)phenyl)diazenyl)phenoxy)ethyl)-2-nitrophenyl)sulfonamido)propyl (7-methyl-1,8-naphthyridin-2-yl)carbamate (10)

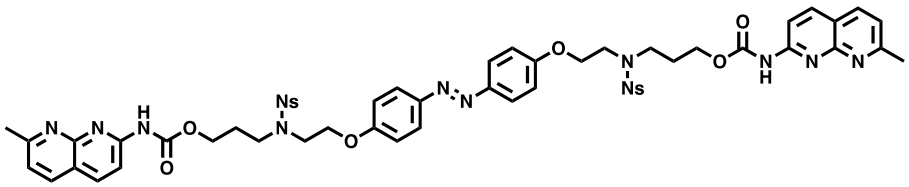

To a solution of **7** (32.0 mg, 0.075 mmol) in anhydrous *N*, *N*-dimethylformamide (DMF, 1 mL) were successively added **9** (112.0 mg, 0.25 mmol)[2] and K_2CO_3 (107.2 mg, 0.78 mmol), and the mixture was stirred at ambient temperature for 3 d. The reaction mixture was diluted with $NaHCO_3$ (sat., aq.) and extracted with EtOAc. The organic layer was successively dried over $MgSO_4$, filtered, and evaporated *in vacuo*. The crude product was purified by column chromatography on silica gel ($CHCl_3$ / MeOH = 10:1) to give **10** (52.4 mg, 0.045 mmol, 61%) as a yellow solid. ^{1}H NMR ($CDCl_3$, 400 MHz) δ = 8.18 (d, J = 8.8 Hz, 2H), 8.11-8.03 (4H), 7.95 (d, J = 8.0 Hz, 2H), 7.77 (d, J = 9.2 Hz, 4H), 7.71 (br, 2H), 7.68-7.59 (6H), 7.23 (J = 8.0 Hz, 2H), 6.87 (d, J = 8.9 Hz, 4H), 4.26 (t, J = 6.0 Hz, 4H), 4.22 (t, J = 5.2 Hz, 3H), 3.80 (t, J = 5.1 Hz, 4H), 3.59 (t, J = 7.0 Hz, 4H), 2.73 (s, 6H), 2.14-2.07 (m, 4H); ^{13}C NMR ($CDCl_3$, 100 MHz) δ = 163.3, 160.0, 154.7, 153.2, 152.9, 148.2, 147.3, 139.2, 136.5, 133.8, 133.1, 131.9, 131.0, 124.5, 124.4, 121.5, 118.1, 114.6, 112.6, 67.2, 63.0, 47.1, 46.2, 27.7, 25.7; ESI-MS *m/z*: calcd. For $[C_{54}H_{52}N_{12}O_{14}S_2 + Na]^+$ 1179.31; found 1179.05.

(E)-((((diazene-1,2-diylbis(4,1-phenylene))bis(oxy))bis(ethane-2,1-diyl))bis(azanediyl))bis(propane-3,1-diyl) bis((7-methyl-1,8-naphthyridin-2-yl)carbamate) (2)

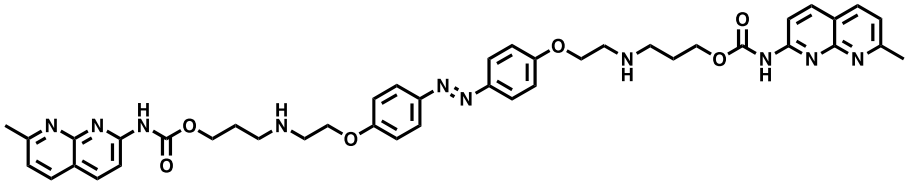

To a solution of **10** (6.4 mg, 5.5 μmol) in anhydrous *N*, *N*-dimethylformamide (DMF, 0.5 mL) were successively added benzenethiol (2.40 mg, 0.02 mmol) and K_2CO_3 (12.2 mg, 0.09 mmol), and the mixture was stirred at ambient temperature for 1 h. The reaction mixture was diluted with saturated $NaHCO_3$ and extracted with EtOAc. The organic layer was successively dried over $MgSO_4$, filtered, and the solvent was evaporated *in vacuo*. The residue was purified by column chromatography on silica gel ($CHCl_3$ / MeOH = 100:1 to 4:1) to give **2** (2.7 mg, 3.4 μmol, 62%) as a yellow powder. Compound **2** in CD_3OD exists as a 91 : 9 mixture of *E* : *Z* isomer and the following NMR spectrum was reported for the *E* isomer unless noted. ^{1}H NMR

(CD_3OD, 700 MHz) δ = 8.85 (d, J = 8.0 Hz, 2H), 8.58 (d, J = 9.3 Hz, 2H), 8.52 (d, J = 9.0 Hz, 2H), 7.77-7.76 (m, 4H), 7.73 (d, J = 8.3 Hz, 2H), 7.16 (d, J = 7.1 Hz, 4H), 6.95 (d, J = 9.0 Hz, 4H for *Z* isomer), 6.86 (d, J = 9.0 Hz, 4H for *Z* isomer), 4.44 (t, J = 5.0 Hz, 4H), 4.42 (t, J = 6.1 Hz, 4H), 3.59 (t, J = 4.8 Hz, 4H), 3.35-3.33 (m, 4H), 2.91 (s, 6H), 2.25-2.21 (m, 4H); ^{13}C NMR (CD_3OD, 176 MHz) δ = 160.0, 159.3, 157.8, 153.2, 147.4, 147.2, 146.0, 139.7, 124.1, 121.7, 119.5, 116.0, 114.7, 63.3, 62.5, 46.6, 44.7, 25.4, 19.2; ESI-MS *m/z*: calcd. For $[C_{42}H_{46}N_{10}O_6 + H]^+$ 787.3675; found 787.3651.

(*E*)-1,2-bis(4-(3-bromopropoxy)phenyl)diazene (8)

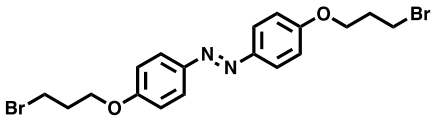

To a solution of anhydrous potassium carbonate (516 mg, 3.73 mmol) in dry DMF (2 mL) was added 4,4'-dihydroxyazobenzene **6** (77.4 mg, 0.37 mmol). After stirred for 30 min, dibromopropane (739 mg, 3.73 mmol) was added, and the solution was then stirred for 24 h before the reaction mixture was poured into water. The mixture was extracted with EtOAc. The yellow organic phase was washed with water several times, dried over by anhydrous Na_2SO_4 and the solvent was removed under reduced pressure. Then the solid residue was recrystallized from $CHCl_3$ / MeOH to give **8** (92.8 mg, 0.20 mmol, 56%) as a yellow powder. ^{1}H NMR ($CDCl_3$, 400 MHz) δ = 7.87 (d, J = 8.8 Hz, 4H), 7.01 (d, J = 9.2 Hz, 4H), 4.19 (t, J = 5.8 Hz, 4H), 3.63 (t, J = 6.4 Hz, 4H), 2.37 (m, 4H).

(*E*)-3-((N-(3-(4-((4-(3-((N-(3-(((7-methyl-1,8-naphthyridin-2-yl)carbamoyl)oxy)propyl)-2-nitrophenyl)sulfonamido)propoxy)phenyl)diazenyl)phenoxy)propyl)-2-nitrophenyl) sulfonamido)propyl (7-methyl-1,8-naphthyridin-2-yl)carbamate (11)

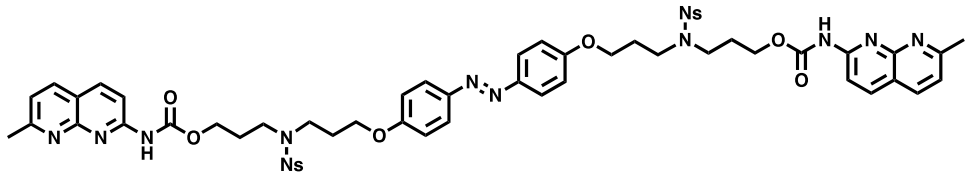

To a solution of **8** (21.0 mg, 0.046 mmol) in anhydrous *N*, *N*-dimethylformamide (DMF, 1 mL) were successively added **9** (35.0 mg, 0.079 mmol)[2] and K_2CO_3 (13.6 mg, 0.10 mmol), and the mixture was stirred at ambient temperature for 1 d. The reaction mixture was diluted with $NaHCO_3$ (sat., aq,.) and extracted with EtOAc. The organic layer was successively dried over $MgSO_4$, filtered, and evaporated *in vacuo*. The crude product was purified by column chromatography on silica gel ($CHCl_3$ / MeOH = 100:1) to give **11** (16.3 mg, 0.014 mmol, 30%) as a yellow solid. ^{1}H NMR ($CDCl_3$, 400 MHz) δ = 8.21 (d, J = 8.8 Hz, 2H), 8.11 (d, J = 8.8 Hz, 2H), 8.04 (d, J = 7.4 Hz, 2H), 7.98 (d, J = 8.2 Hz, 2H), 7.81-7.77 (m, 4H), 7.73 (br, 2H), 7.61-7.53 (6H), 7.26 (d, J = 8.0 Hz, 2H), 6.88-6.84 (m, 4H), 4.26 (t, J = 6.1 Hz, 4H), 4.00 (t, J = 5.7 Hz, 4H), 3.59 (t, J = 7.0 Hz, 4H), 3.52 (t, J = 7.2 Hz, 4H), 2.75 (s, 6H), 2.11-2.01 (8H); ^{13}C NMR ($CDCl_3$, 100 MHz) δ = 163.4, 160.5, 154.7, 153.2, 152.9, 148.0, 147.1, 139.2, 136.5, 133.7, 133.0, 131.8, 131.1, 124.4, 124.3, 121.5, 118.1, 114.6, 112.6, 64.8, 63.0, 44.3, 44.2, 27.9, 27.5, 25.7; ESI-MS *m/z*: calcd. For $[C_{56}H_{56}N_{12}O_{14}S_2 + H]^+$ 1184.35; found 1184.34.

(*E*)-((((diazene-1,2-diylbis(4,1-phenylene))bis(oxy))bis(propane-3,1-diyl))bis(azanediyl)) bis(propane-3,1-diyl) bis((7-methyl-1,8-naphthyridin-2-yl)carbamate) (3)

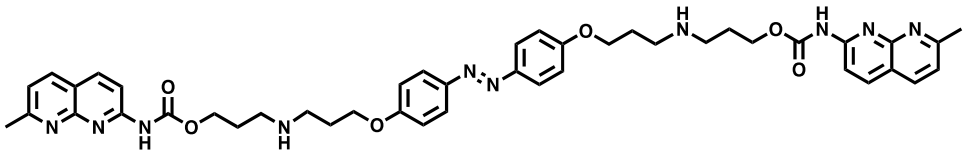

To a solution of **11** (22.1 mg, 0.019 mmol) in anhydrous *N*, *N*-dimethylformamide (DMF, 1 mL) were successively added benzenethiol (8.30 mg, 0.075 mmol) and K_2CO_3 (36.0 mg, 0.26 mmol), and the mixture was stirred at ambient temperature for 1 h. The reaction mixture was diluted with $NaHCO_3$ (sat., aq.) and extracted with EtOAc. The organic layer was successively dried over $MgSO_4$, filtered, and the solvent was evaporated *in vacuo*. The residue was added HCl (4M, aq.) and the reaction mixture was extracted with EtOAc. The water layer was diluted with $NaHCO_3$ (sat., aq.) and extracted with EtOAc. The crude product was purified by HPLC to give **3** (12.0 mg, 0.015 mmol, 79%) as a yellow solid. Compound **3** in CD_3OD exists as a 85 : 15 mixture of *E* : *Z* isomer and the following NMR spectrum is reported for *E* isomer unless noted. ^{1}H NMR (CD_3OD, 700 MHz) δ = 8.86 (d, *J* = 8.2 Hz, 2H), 8.58 (d, *J* = 9.0 Hz, 2H), 8.52 (d, *J* = 9.0 Hz, 2H), 7.78 (d, *J* = 9.0 Hz, 4H), 7.76 (d, *J* = 8.6 Hz, 2H), 7.09 (d, *J* = 9.0 Hz, 4H), 6.90 (8H for *Z* isomer), 4.40 (t, J = 6.0 Hz, 4H), 4.25 (t, *J* = 5.6 Hz, 4H), 3.33 (t, *J* = 7.3 Hz, 4H), 3.27 (t, *J* = 7.5 Hz, 4H), 2.94 (s, 6H), 2.30-2.26 (m, 4H), 2.22-2.18 (m, 4H); ^{13}C NMR (CD_3OD, 176 MHz) δ = 160.7, 159.4, 157.8, 153.1, 147.4, 147.0, 146.1, 139.8, 124.0, 121.8, 119.6, 116.1, 114.5, 65.2, 62.8, 45.5, 45.0, 25.8, 25.5, 19.3; ESI-MS *m/z*: calcd. For $[C_{44}H_{50}N_{10}O_6 + H]^+$ 815.3988; found 815.3951.

Route 2: Reductive Amination as Key Step

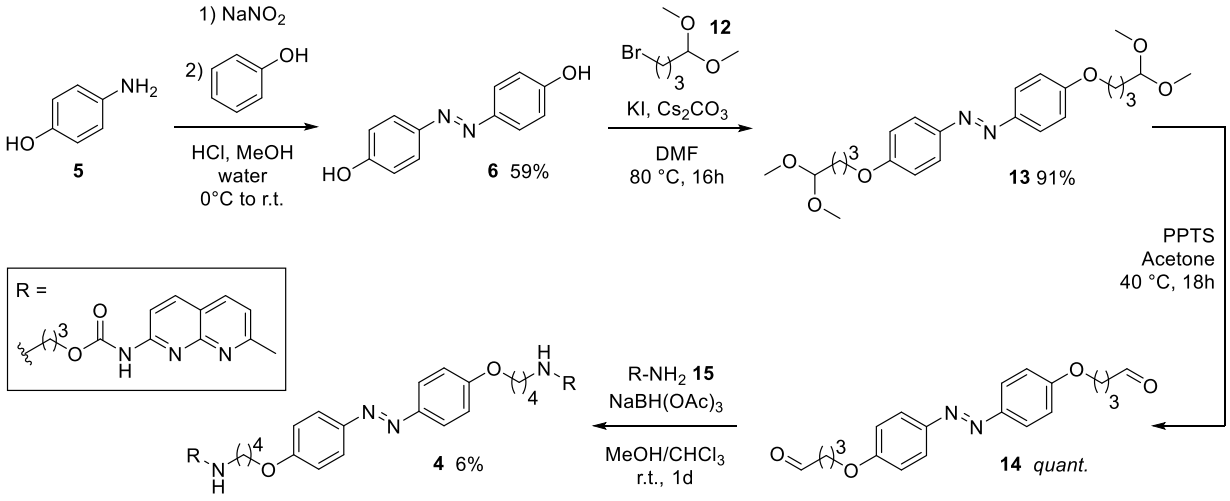

Scheme S2. Synthesis of target compound **4** *via* reductive amination as key step.

Alkylation of **6** with **12** was facilitated using Cs_2CO_3 in DMF to give compound **13**. Deprotection of the aldehyde functionalities was achieved quantitatively with pyridinium *p*-toluenesulfonate (PPTS). Target compound **4** could be successfully synthesized *via* reductive amination treating **14** with $NaBH(OAc)_3$ and the corresponding amine **15** (Scheme S2).

(*E*)-1,2-bis(4-(4,4-dimethoxybutoxy)phenyl)diazene (13)

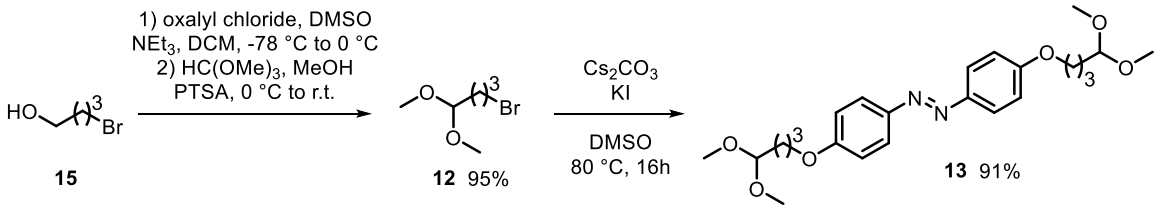

Acetal **12** was synthesized following a published protocol employing 4-bromo butanol (**15**, 800 mg, 5.23 mmol) and was isolated in 95% yield and used in the next step without further purification. ^{1}H NMR (400 MHz, Chloroform-*d*) δ = 4.39 (t, *J* = 5.6 Hz, 1H), 3.43 (t, *J* = 6.7 Hz, 2H), 3.32 (s, 6H), 2.00 – 1.85 (m, 2H), 1.79 – 1.71 (m, 2H). The analytical data were in agreement with published data.[3]

Compound **6** (150 mg, 0.70 mmol), Cs_2CO_3 (913 mg, 2.8 mmol), and KI (12 mg, 0.07 mmol) were added to a Schlenk flask under nitrogen and dissolved in dry DMSO (5 mL). The reaction mixture was heated at 80 °C for 15 min and cooled to ambient temperature. Then, acetal **12** (275 mg, 1.40 mmol) was added and the resulting mixture was stirred at 80 °C for 16 h. The solution was cooled to ambient temperature and diluted with water (150 mL) and EtOAc (60 mL). The phases were separated, and the organic phase was washed with water (100 mL) and brine (80 mL) and dried over Na_2SO_4. The volatiles were removed *in vacuo* to give the title compound as an orange solid (285 mg, 0.64 mmol, 91%). ^{1}H NMR (400 MHz, Acetone-d_6) δ = 7.87 (d, *J* = 8.9 Hz, 4H), 7.09 (d, *J* = 8.8 Hz, 4H), 4.45 (t, *J* = 5.4 Hz, 2H), 4.13 (t, *J* = 6.3 Hz, 4H), 3.29 (s, 12H), 1.96 – 1.81 (m, 4H), 1.77 (dt, *J* = 10.8, 5.7 Hz, 4H). ^{13}C NMR (101 MHz, Acetone-d_6) δ = 161.3 (q), 146.8 (q), 124.2 (+), 114.7 (+), 104.1 (+), 67.8 (-), 52.0 (+), 28.9 (-), 24.3 (-). IR [cm^{-1}] (*neat*) = 2956 (m), 1595 (s), 1500 (s), 1467 (m), 1393 (m), 1251 (s), 1128 (s), 842 (s), 735 (m), 553 (m). The compound could not be ionized in MS spectroscopy. Mp: 82-85 °C. R_f: 0.8 (pentante : EtOAc = 1:1 (v/v).

(*E*)-4,4'-((diazene-1,2-diylbis(4,1-phenylene))bis(oxy))dibutanal (14)

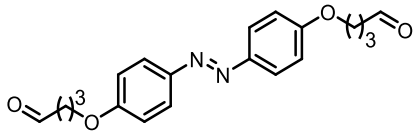

Acetal **7** (10.0 mg, 22.4 µmol) was dissolved in acetone (300 µL) and pyridinium *p*-toluene sulfonate (PTSA, 1.7 mg, 6.7 µmol) was added. The solution was warmed to 40 °C for 18h and then cooled to ambient temperature. The reaction mixture was filtered over a plug of celite using acetone as an eluent to remove PTSA. The volatiles were removed *in vacuo* to give a dark yellow solid (7.9 mg, 22.3 µmol, *quant.*). The identity of the compound was confirmed by ^{1}H spectroscopy, and the title compound was converted without further purification. ^{1}H NMR (400 MHz, Acetone-d_6) δ = 9.82 (t, *J* = 1.3 Hz, 2H), 7.98 – 7.77 (m, 4H), 7.14 – 7.05 (m, 4H), 4.15 (t, *J* = 6.3 Hz, 4H), 2.69 (td, *J* = 7.1, 1.3 Hz, 4H), 2.17 – 2.11 (m, 4H). R_f: 0.3 (pentane : EtOAc = 1:1 (v/v).

(*E*)-3-((4-(4-((4-(3-((3-(((7-methyl-1,8-naphthyridin-2-yl)carbamoyl)oxy)propyl)amino) propoxy)phenyl)diazenyl)phenoxy)butyl)amino)propyl (7-methyl-1,8-naphthyridin-2-yl)carbamate (4)

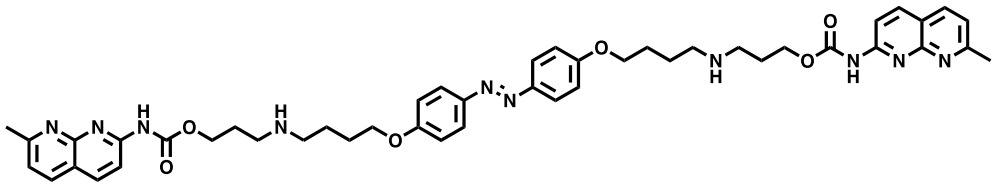

To a mixture of **14** (30.0 mg, 0.085 mmol) and **15** (43.7 mg, 0.17 mmol)[4] in $CHCl_3$ (7 mL) was added acetic acid (25 μL, 0.43 × 10^{-3} mmol) and the reaction mixture was stirred at ambient temperature for 30 min. Sodium triacetoxyborohydride (189 mg, 0.90 mmol) in methanol (3 mL) was added to the reaction mixture. After 16 h stirring, the solvent was removed *in vacuo* and the residue was diluted with saturated aqueous $NaHCO_3$ solution and extracted with EtOAc. The organic phase was washed with brine, dried over anhydrous $MgSO_4$, filtered, and concentrated *in vacuo*. Then, 4M hydrochloric acid was added to the residue. The reaction mixture was extracted with EtOAc. The water layer was diluted with $NaHCO_3$ (sat, aq.) and extracted with EtOAc. The crude product was purified by HPLC to give **4** (4.3 mg, 0.005 mmol, 6%) as a yellow solid. Compound **4** in CD_3OD exists as a 84 : 16 mixture of *E* : *Z* isomer and the following NMR spectrum was reported for *E* isomer unless noted. ^{1}H NMR (CD_3OD, 700 MHz) δ = 8.77 (br, 2H), 8.54 (d, *J* = 9.3 Hz, 2H), 8.49 (d, *J* = 9.0 Hz, 2H), 7.81 (d, *J* = 9.0 Hz, 4H), 7.72 (d, *J* = 8.0 Hz, 2H), 7.05 (d, *J* = 9.0 Hz, 4H), 6.87 (d, *J* = 9.0 Hz, 4H for *Z* isomer), 6.84 (d, *J* = 9.3 Hz, 4H for *Z* isomer), 4.39 (t, *J* = 6.1 Hz, 4H), 4.14 (m, 4H), 3.23 (t, *J* = 7.7 Hz, 4H), 3.18-16 (m, 4H), 2.90 (s, 6H), 2.19-2.15 (m, 4H), 1.97-1.94 (m, 8H); ^{13}C NMR (CD_3OD, 176 MHz) δ = 161.0, 159.9, 158.4, 157.2, 153.2, 146.8, 146.5, 139.7, 123.9, 122.4, 121.7, 119.3, 115.5, 114.4, 67.1, 62.5, 44.7, 44.7, 25.9, 25.5, 22.9, 19.9; ESI-MS *m/z*: calcd. For $[C_{46}H_{54}N_{10}O_6 + Na]^+$ 865.4120; found 865.1820.

2. Photochemical and Thermal Isomerization by UV-Vis and NMR Spectroscopy

UV/Vis absorption spectra were recorded on an Agilent 8453 UV-Visible Spectrophotometer. Photochemical isomerization was achieved by irradiation from the side in a fluorescence quartz cuvette (width = 1.0 cm) using a custom-built (Prizmatix/Mountain Photonics) multi-wavelength fiber coupled LED-system (FC6-LED-WL) including the following LEDs: 365A, 390B, 420Z, 445B, 535R, 630CA. A detailed description of the setup was published in reference 5. A Quantum Northwest TC1 temperature controller was used to maintain the temperature at 25 °C during photochemical studies. Thermal isomerization kinetics were recorded using a JASCO V750 at 25 °C using a PTC 424S/15 temperature controller. Raw data were processed using Agilent UV-Vis ChemStation B.02.01 SP1, Spectra Manager, Spectragryph 1.2, and OriginPro 2016.
For photostationary distribution (PSD) determination by ^{1}H NMR 0.6 mL of a 1 mM solution of the respective compound in D_2O was thermally equilibrated in the dark at 60 °C for 1h, or irradiated in a glass NMR tube using a 365 nm hand-held lamp (Spectroline ENB-280C) or a Sahlmann cooled 3 x Roithner SMB-1N 430h (426 nm, FWHM = 16 nm, power output = 600 mW), respectively.

2.1.UV-Vis spectra at Different Concentration for ε Determination

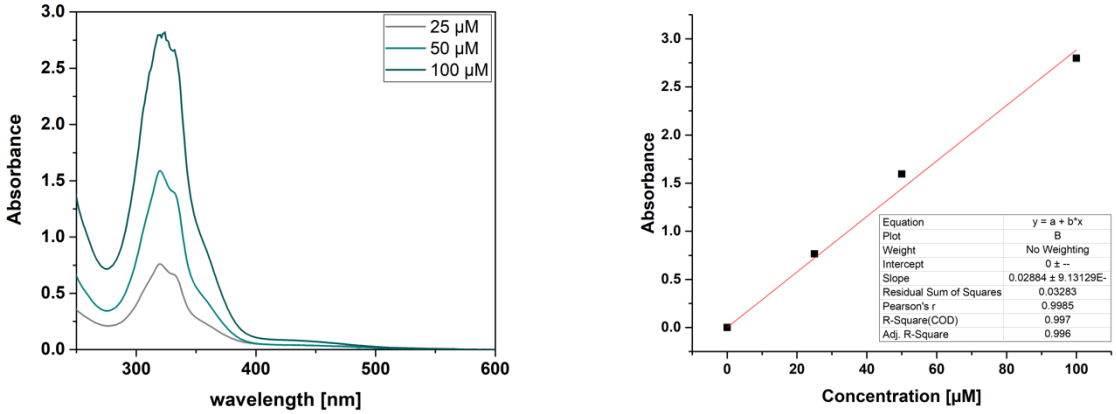

Figure S1. NCDA3 in Tris buffer (aq., 50 mM, 150 mM NaCl, pH = 7.5).

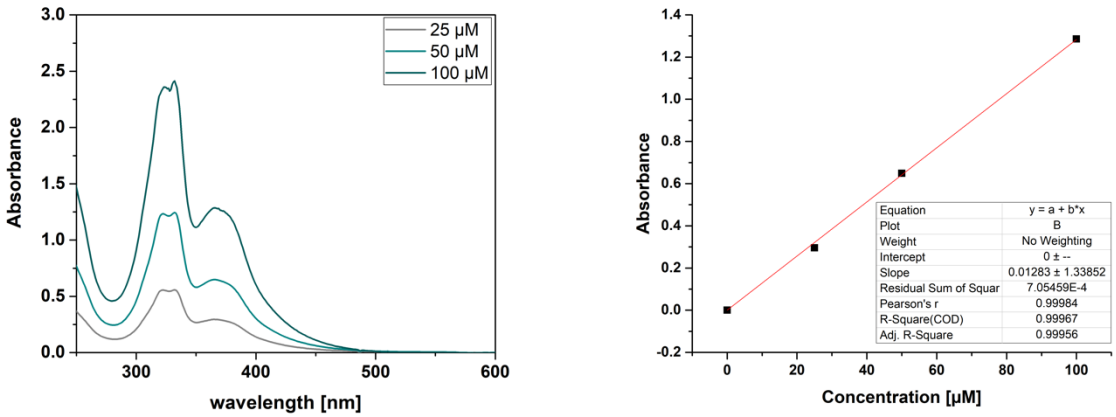

Figure S2. Compound **2** in Tris buffer (aq., 50 mM, 150 mM NaCl, pH = 7.5).

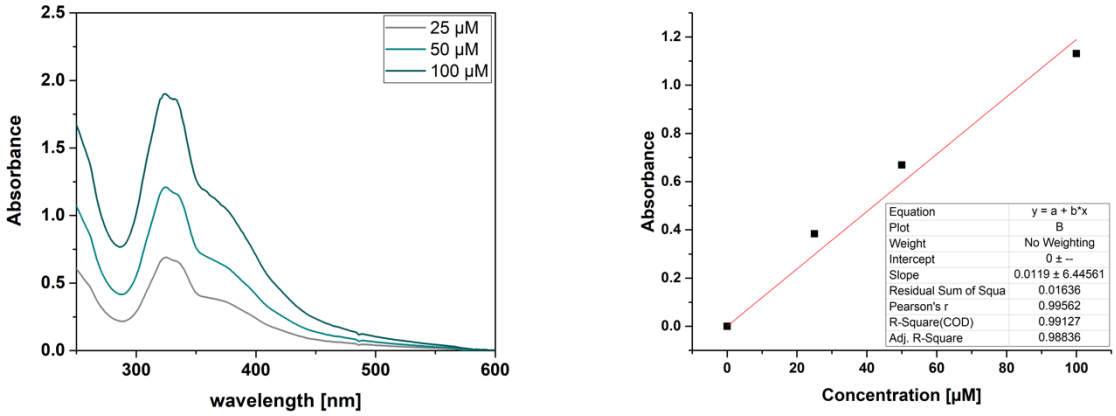

Figure S3. Compound **3** in phosphate buffer (aq., 0.01 M, 100 mM NaCl, pH = 7.0).

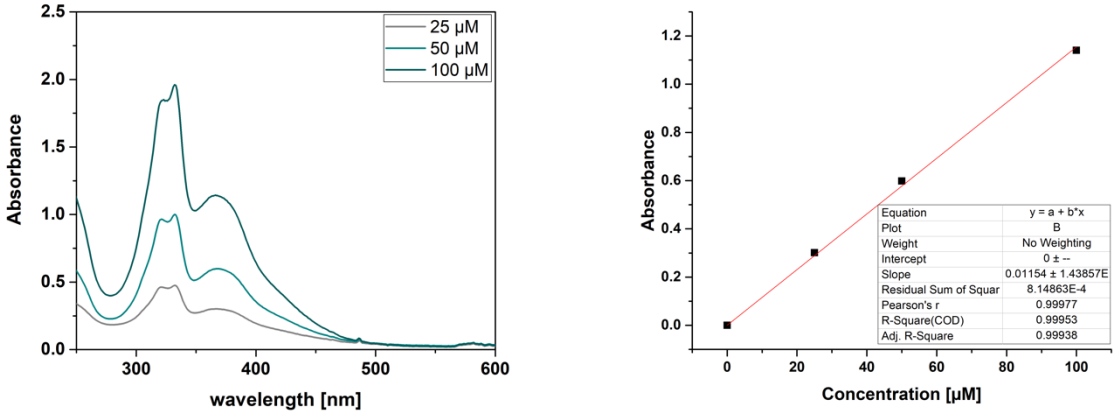

Figure S4. Compound **4** in water.

2.2.Spectra of Photoisomerization

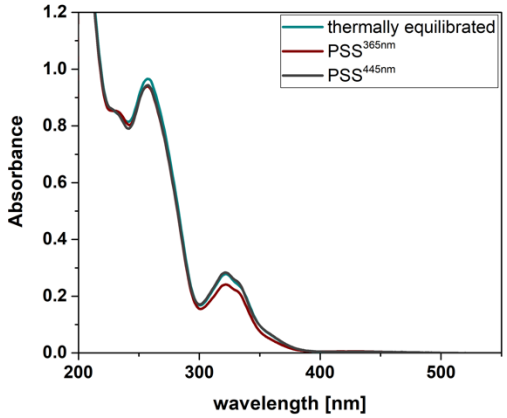

Figure S5. NCDA3 in phosphate buffer (aq., 0.01 M, 100 mM NaCl, pH = 7.0) and dsDNA (5µM). NCDA3 without DNA see main text.

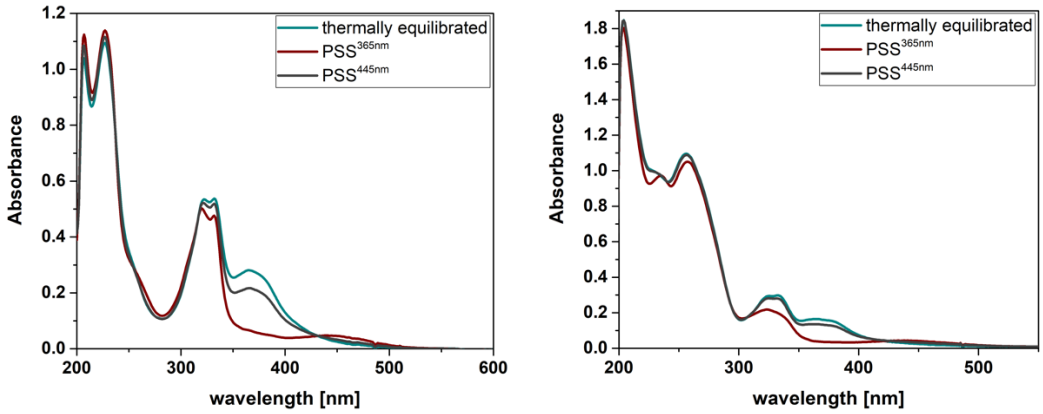

Figure S6. **Left**. Compound **2** in Tris buffer (aq., 50 mM, 150 mM NaCl, pH = 7.5). **Right**. Compound **2** in phosphate buffer (0.01 M, 100 mM NaCl, pH = 7.0) and dsDNA (5µM).

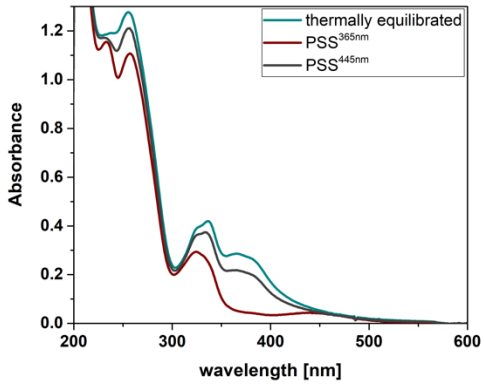

Figure S7. Compound **3** in phosphate buffer (aq., 0.01 M, 100 mM NaCl, pH = 7.0) and dsDNA (5µM). Compound **3** without DNA see main text.

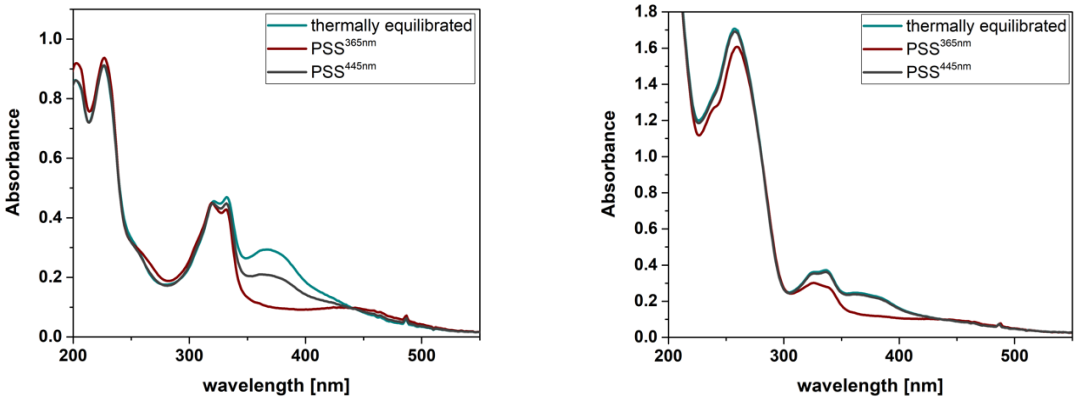

Figure S8. **Left**. Compound **4** in phosphate buffer (aq., 0.01 M, 100 mM NaCl, pH = 7.0). **Right**. Compound **3** in phosphate buffer (aq., 5 mM, 50 mM NaCl, pH = 7.0) and dsDNA (5µM).

2.3.QY Determination

Chemical actinometry. A modification of a standard protocol was applied for the determination of the photon flux.[5] An aqueous H_2SO_4 solution (0.05 M) containing freshly recrystallized $K_3[Fe(C_2O_4)_3]$ (41 mM, 2 mL, 1 cm quartz cuvette) was irradiated at 20 °C for a given period of time in the dark with a 365 nm LED. The solution was then diluted with 1.0 mL of an aqueous H_2SO_4 solution (0.5 M) containing phenanthroline (1 g/L) and NaOAc (122.5 g/L) and left to react for 10 min. The absorption at λ= 510 nm was measured and compared to an identically prepared non-irradiated sample. The concentration of $[Fe(phenanthroline)_3]^{2+}$ complex was calculated using its molar absorptivity (ε = 11100 M^{-1} cm^{-1}) and considering the dilution. The quantity of Fe^{2+} ions expressed in mol was plotted versus time (expressed in seconds) and the slope, obtained by linear fitting the data points to the equation y = ax +b using Origin software, equals the rate of formation of the Fe^{2+} ions at the given wavelength under standardized conditions. This rate can be converted into the photon flux (I) by dividing it by the quantum yield of $[Fe(phenanthroline)_3]^{2+}$ complex ($\Phi^{365nm} = 1.29$)[6] at 365 nm and by the probability of photon absorption at 365 nm of the Fe^{3+} complex (approximated to 1 as the experiment was performed in the total absorption regime). The obtained photon flux was $I = 3.70588 \times 10^{-5}$ E s^{-1}.

Quantum yield measurement. The quantum yields of the compounds were determined by monitoring the decrease of the ππ* transition band at the wavelength of irradiation by UV-Vis spectroscopy (Agilent 8453) following published procedures.[5] Irradiation was performed in quartz fluorescence cuvettes (pathlength = 1 cm) with defined volumes (*vide infra*) using the 365 nm LED of our multi-wavelength fiber coupled LED-system with a defined photon flux (*vide supra*) under stirring at 25 °C.

2.3.1. Without DNA

Table S1. NCDA3, 25 μM in Tris buffer (aq., 50 mM, 150 mM NaCl, pH = 7.5)

NCDA3	
Lambda(nm)	320
Conc	0.000025
Photon flux	3.7059E-05
A	0.8007
Slope	-0.00226
Volume(ml)	2
rate	-5.65E-08
QY	0.00362239

Table S2. Compound **2**, 25 μM in Tris buffer (aq., 50 mM, 150 mM NaCl, pH = 7.5)

Compound2	
Lambda(nm)	365
Conc	0.000025
Photon flux	3.7059E-05
A	0.335
Slope	-0.1675
Volume(ml)	2
rate	-4.1875E-06
QY	0.42035707

Table S3. Compound **3**, 50 μM in phosphate buffer (aq., 0.01 M, 100 mM NaCl, pH = 7.0)

Compound3	
Lambda(nm)	365
Conc	0.00005
Photon flux	3.7059E-05
A	0.567
Slope	-0.14339
Volume(ml)	2
rate	-7.1695E-06
QY	0.53077552

Table S4. Compound **4**, 25 μM in water

Lambda(nm)	365
Conc	2.50E-05
Photon flux	3.71E-05
A	0.30127
Slope	-0.0985
Volume(ml)	2
rate	-2.4625E-06
QY	0.26564674

2.3.2. With dsDNA

Table S5. NCDA3, 10 μM in phosphate buffer (aq., 0.01 M, 100 mM NaCl, pH = 7.0, with 5 μM dsDNA)

NCDA3	
Lambda(nm)	321
Conc	0.00001
Photon flux	3.7059E-05
A	0.2872
Slope	-0.00933
Volume(ml)	2
rate	-9.33E-08
QY	0.01040722

Table S6. Compound **2**, 10 μM in phosphate buffer (aq., 0.01 M, 100 mM NaCl, pH = 7.0, with 5 μM dsDNA)

Compound2	
Lambda(nm)	365
Conc	0.00001
Photon flux	3.7059E-05
A	0.1792
Slope	-0.0934
Volume(ml)	2
rate	-9.34E-07
QY	0.14909214

Table S7. Compound **3**, 20 μM in phosphate buffer (aq., 0.01 M, 100 mM NaCl, pH = 7.0, with 10 μM dsDNA)

Compound3	
Lambda(nm)	367
Conc	0.00002
Photon flux	3.7059E-05
A	0.3444
Slope	-0.05701
Volume(ml)	2
rate	-1.1402E-06
QY	0.11238793

Table S8. Compound **4**, 24μM in phosphate buffer (aq., 0.01 M, 100 mM NaCl, pH = 7.0, with 5 μM dsDNA)

Lambda(nm)	367
Conc	2.40E-05
Photon flux	3.71E-05
A	0.17419
Slope	-0.03592
Volume(ml)	1.9
rate	-8.6208E-07
QY	0.13376985

2.4.Switching Cycles for Fatigue (with and without DNA)

To analyze the fatigue resistance of compounds **2**-**4**, we performed repeated irradiation cycles using alternating 365 nm and 445 nm light. The decrease and increase of the ππ* transition band was followed by UV-Vis spectroscopy (Agilent 8453) at 25 °C. The obtained data is depicted below.

2.4.1. Compound **2**, λ^{obs}=365 nm

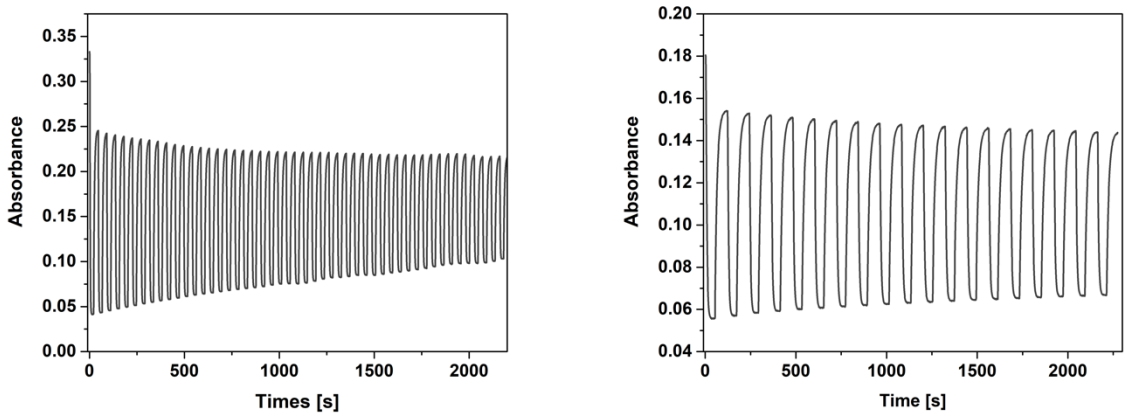

Figure S9. Left: 25 μM in Tris buffer (aq., 50 mM, 150 mM NaCl, pH = 7.5); Right: 10 μM in phosphate buffer (0.01 M, 100 mM NaCl, pH = 7.0, with 5 μM dsDNA).

2.4.2. Compound **3**

Data for compound **3** see main text

2.4.3. Compound **4**, λ^{obs}=367 nm

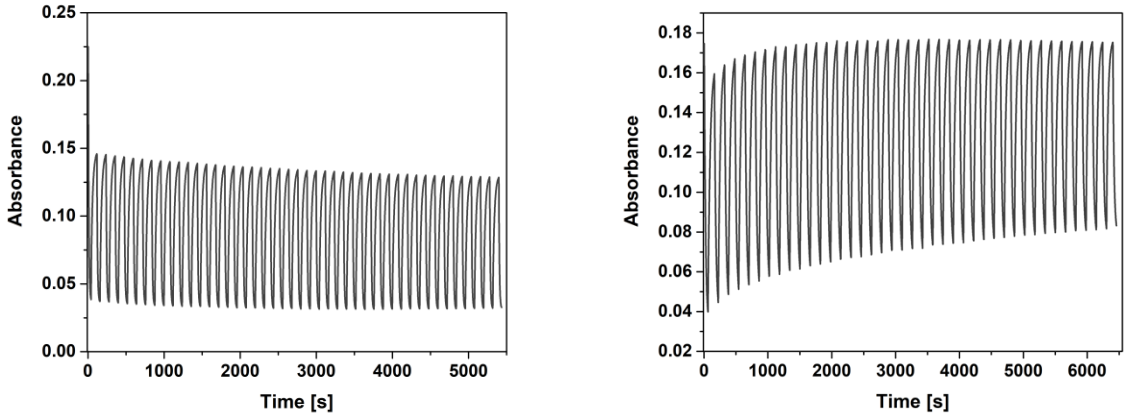

Figure S10. Left: 25 μM in Tris buffer (aq., 50 mM, 150 mM NaCl, pH = 7.5); Right: 10 μM in phosphate buffer (0.01 M, 100 mM NaCl, pH = 7.0, with 5 μM dsDNA).

2.5.Thermal Lifetime τ of *Z* Isomer (with and without DNA)

Samples were prepared and irradiated with a 365 nm hand-held lamp (Spectroline ENB-280C) at the final concentration until PSS was reached. Then, the cuvettes were placed in a JASCO V750 spectrophotometer and the appearance of the ππ* transition (or λ_{max} for NCDA3) was followed while stirring at 25 C. The data were fitted using a first-order exponential function in OriginPro 2016.

2.5.1. Without DNA

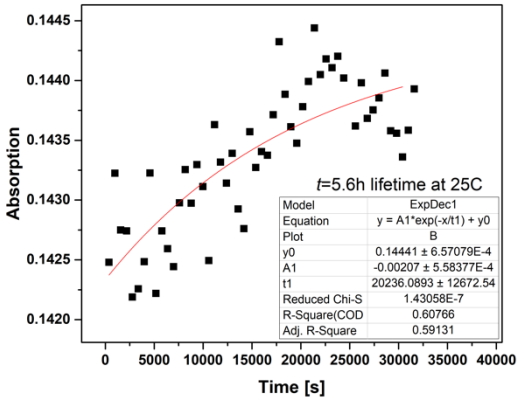

Figure S11. NCDA3, 10 µM in Tris buffer (aq., 50 mM, 150 mM NaCl, pH = 7.5). The scattering in the measurement is cause by the very small difference in absorbance between PSS^{365} and the thermal equilibrium.

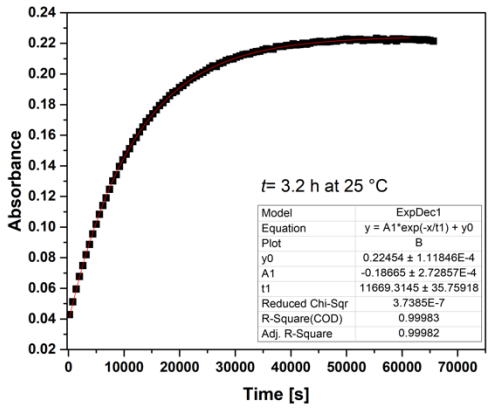

Figure S12. Compound **2**, 10 µM in phosphate buffer (aq., 0.01 M, 100 mM NaCl, pH = 7.0).

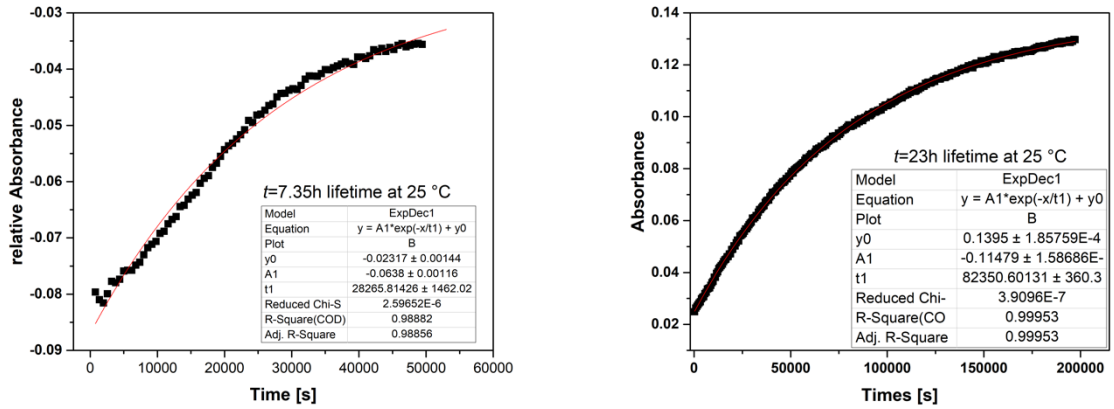

Figure S13. Compound **3**, 10 µM in phosphate buffer (aq., 0.01 M, 100 mM NaCl, pH = 7.0).

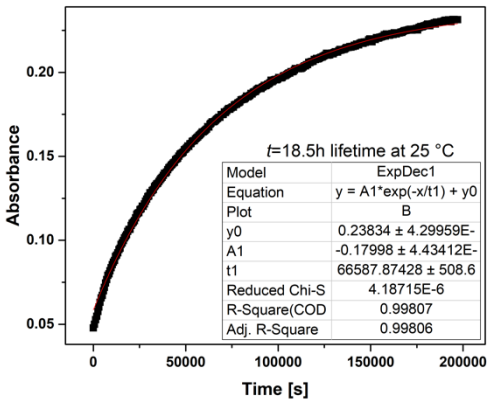

Figure S14. Compound **4**, 10 µM in water.

2.5.2. With dsDNA

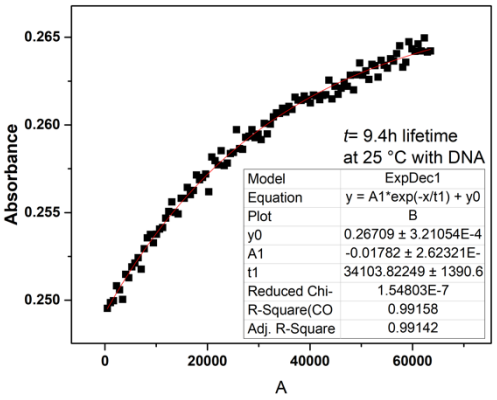

Figure S15. NCDA3, 10 µM in phosphate buffer (aq., 0.01 M, 100 mM NaCl, pH = 7.0), 5µM dsDNA.

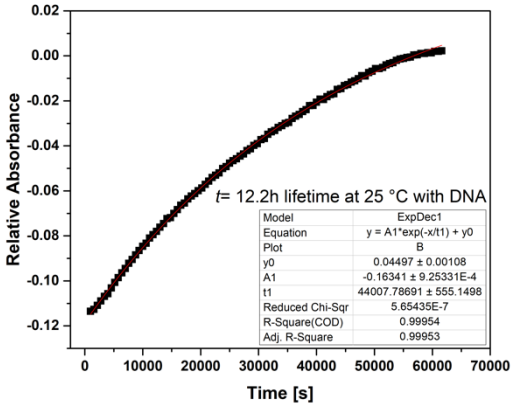

Figure S16. Compound **2**, 10 µM in phosphate buffer (aq., 0.01 M, 100 mM NaCl, pH = 7.0), 5µM dsDNA.

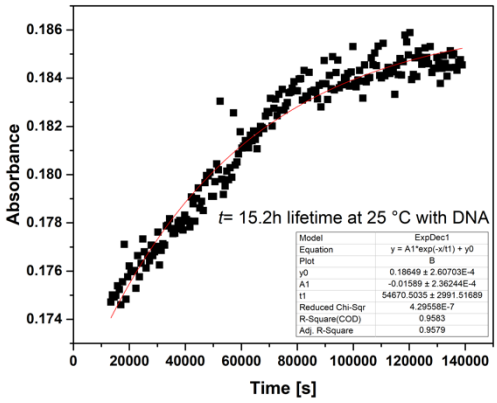

Figure S17. Compound **3**, 10 µM in phosphate buffer (aq., 0.01 M, 100 mM NaCl, pH = 7.0), 5µM dsDNA.

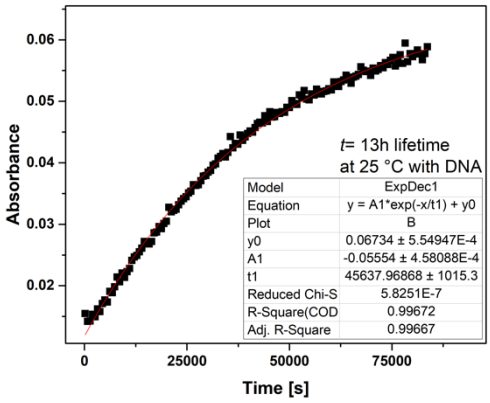

Figure S18. Compound **4**, 10 µM in phosphate buffer (aq., 0.01 M, 100 mM NaCl, pH = 7.0) and water (1:1), 5µM dsDNA.

2.6.PSD Determination by NMR

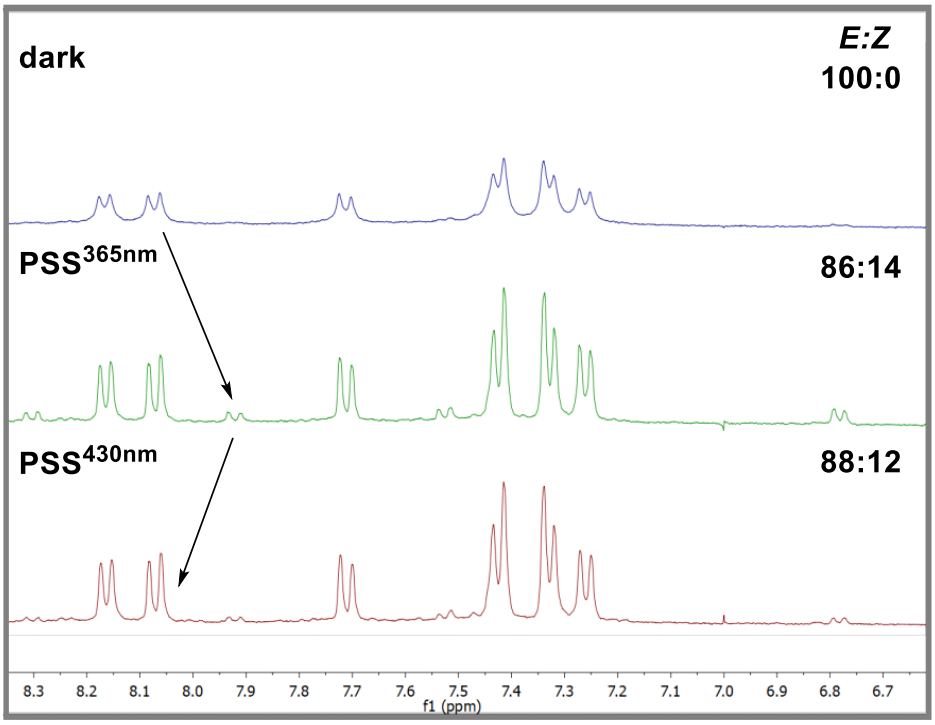

Figure S19. NCDA3, D_2O, 1 mM.

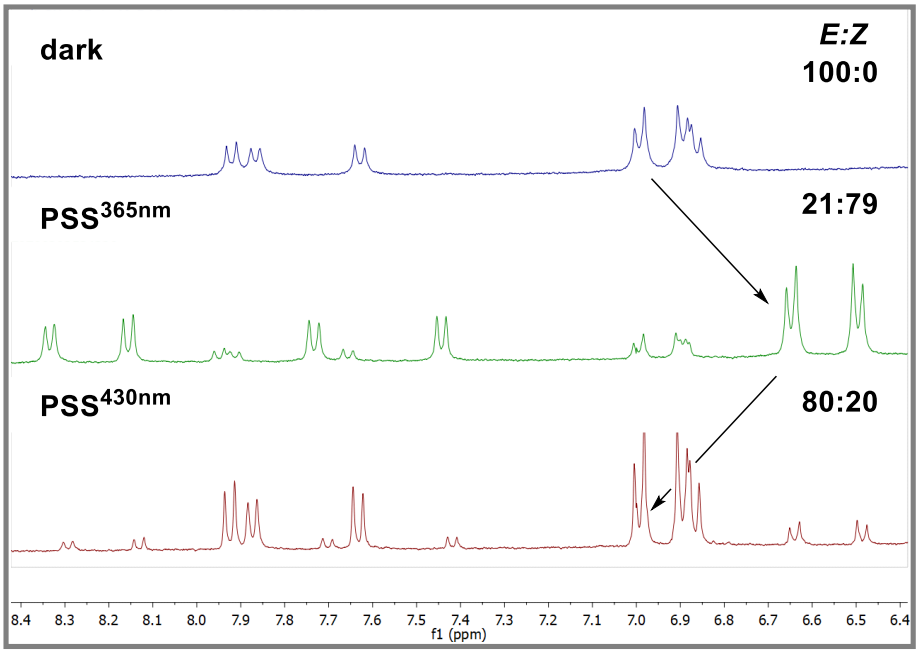

Figure S20. Compound **2**, D_2O, 1 mM.

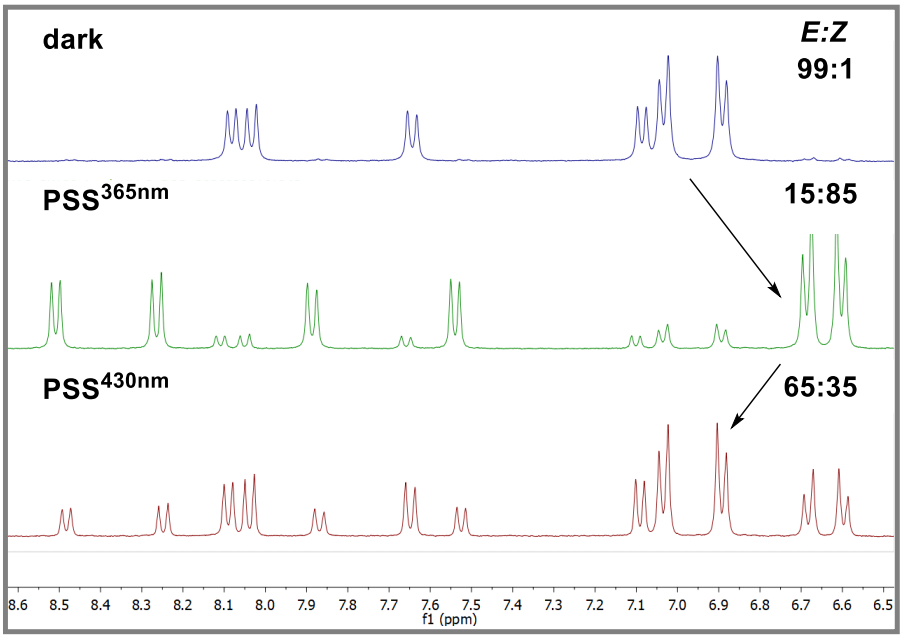

Figure S21. Compound **3**, D_2O, 1 mM.

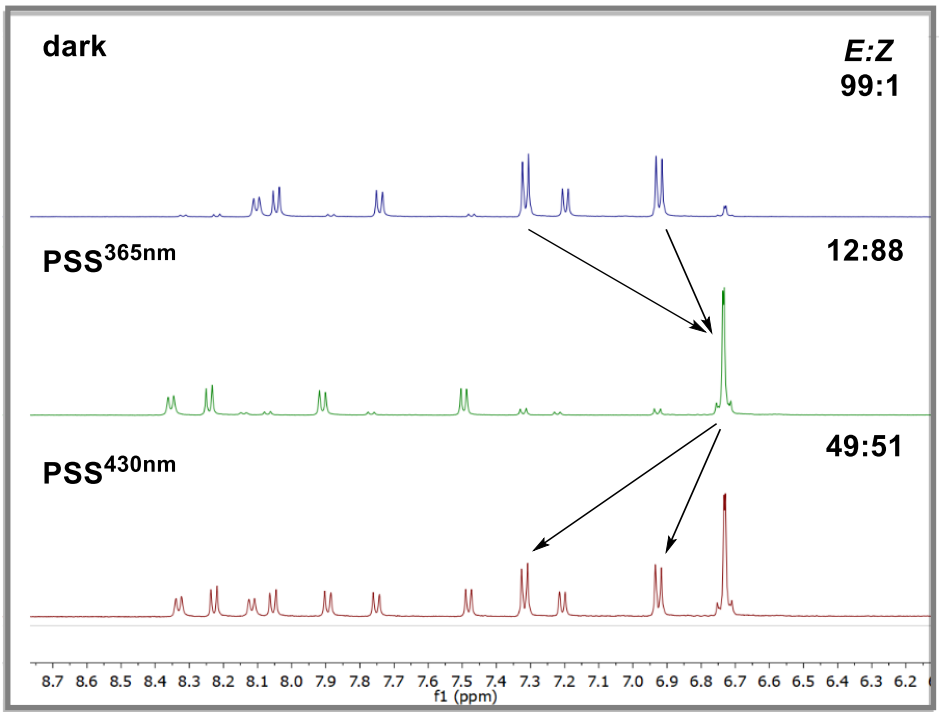

Figure S22. Compound **4**, D_2O, 1 mM.

2.7. PSD Determination by HPLC

2.7.1. Without DNA

A solution containing **2**, **3**, **4** (20 μM) in a phosphate buffer (aq., 10 mM, pH 7.0) containing NaCl (100 mM) was prepared for HPLC analyses. Samples at the photostationary state at 365 nm (PSS^{365nm}) and 460 nm (PSS^{460nm}) light were prepared by photoirradiation with a light source, ZUV-C20H (365 nm, for 20 sec) and UHP-Black-LED-460 (460 nm, for 10 min) at a distance of 10 cm, respectively. Thermally adapted samples were prepared by incubation at 60 ˚C for 1 h under dark condition. The sample solutions were analyzed by reversed phase HPLC (JASCO HPLC system consisting of PU-2084 Quaternary gradient pump and MD-2010 Multiwavelength detector) equipped with COSMOSIL packed column (4.6 × 150 mm)) detected at 251 nm (the wavelength of the isosbestic point); elution with a solvent mixture of 0.1% acetic acid and 0–30% acetonitrile in water (linear gradient for 30 min) at a flow rate 1.0 mL/min.

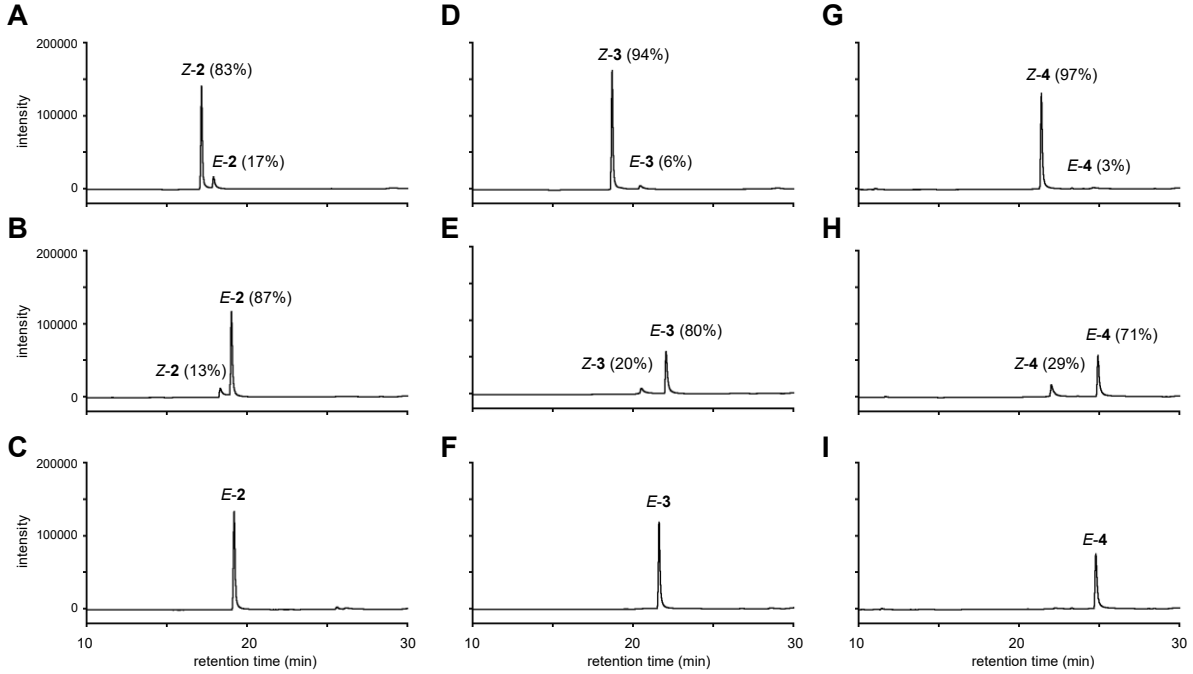

Figure S23. *E-Z* ratio of compounds **2** (**A**–**C**), **3** (**D**–**F**), and **4** (**G**–**I**) at the photostationary state determined by HPLC analyses. **A**, **D**, and **G**. HPLC profiles of compounds at the PSS^{365nm}. **B**, **E**, and **H**. HPLC profiles of compounds at the PSS^{460nm}. **C**, **F**, and **I**. HPLC profiles of the thermally adapted samples.

2.7.2. With DNA

A solution containing **2**, **3**, **4** (200 μM) in phosphate buffer (0.01 M, 100 mM NaCl, pH = 7.0), 5μM dsDNA was prepared for HPLC analyses. Samples at the photostationary state at 365 nm (PSS^{365nm}), 430 nm (PSS^{430nm}) and 470 nm (PSS^{470nm}) light were prepared by photoirradiation with a light source, 365 nm hand-held lamp (Spectroline ENB-280C), or a Sahlmann cooled 3 x Roithner SMB-1N 430h (426 nm, FWHM = 16 nm, power output = 600 mW), or a Sahlmann cooled 3 x Nichia NCSB219B-V1 (464 nm, FWHM = 28 nm, power output = 1000 mW), respectively, at 1 cm distance for 3 min each. Thermally adapted samples were prepared by incubation at 60 ˚C for 1 h under dark conditions. The sample solutions were analyzed by reversed phase HPLC (Shimadzu UFLC system with a SPD-M20A photodiode array detector)

equipped with XTerra®MS C18 3.5 µm packed column (3.0 × 150 mm)) detected at 251 nm (the wavelength of the isosbestic point); elution with a solvent mixture of 0.1% formic acid and 20% acetonitrile (isocratic for 8 min (MBL **2** and **3**) or 18 min (MBL **4**), respectively) at a flow rate 0.5 mL/min. The isomers were identified via the UV-Vis spectrum. The additional signal present in a part of the traces is a result of the injection containing residual DNA.

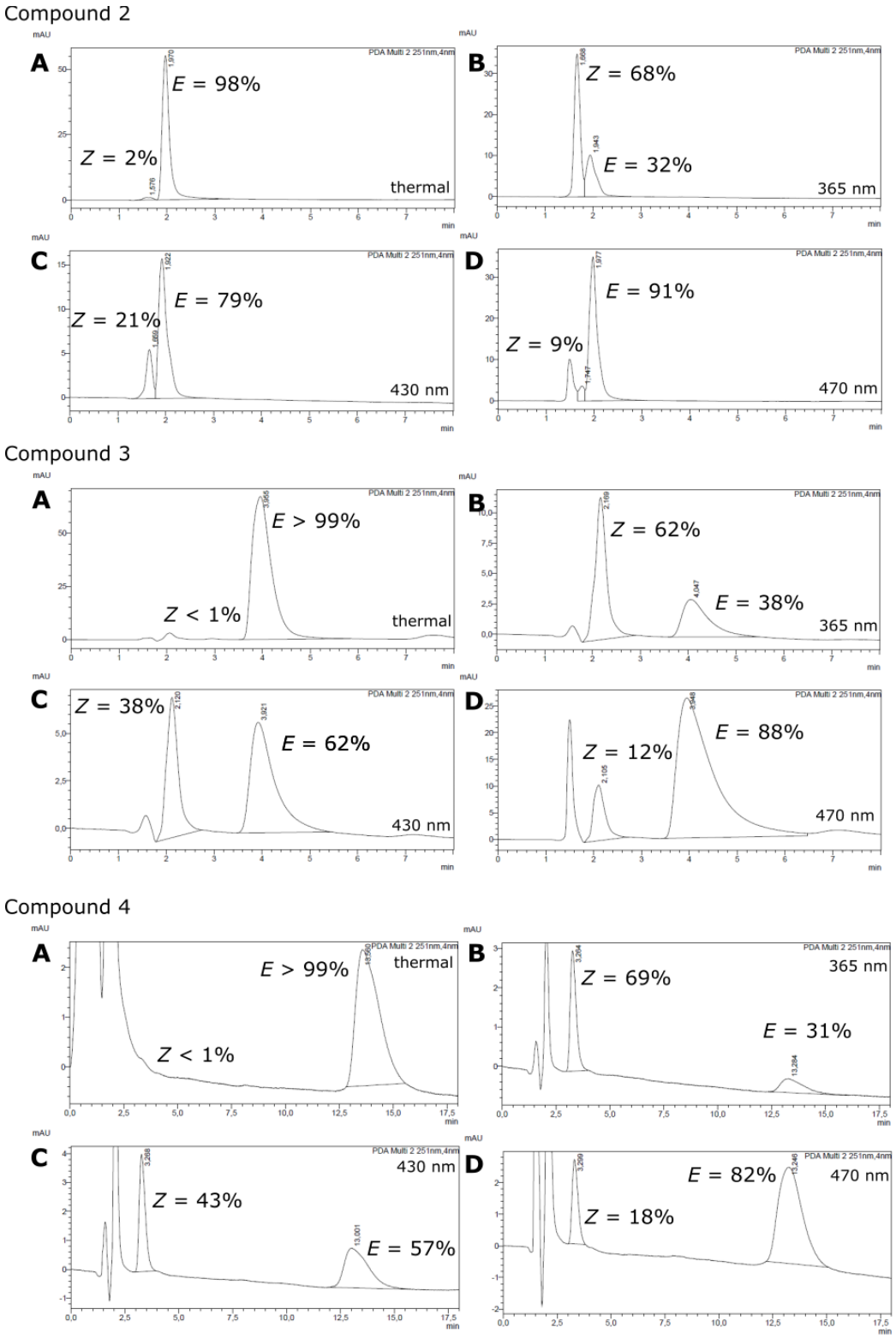

Figure S24. *E-Z* ratio of compounds **2**, **3**, and **4** (top to bottom): HPLC traced at 251 nm at the thermal equilibrium **3** (**A**), the PSS^{365nm} (**B**), the PSS^{430nm} (**C**), and the PSS^{470nm} (**D**).

3. DNA-Melting Experiments

Sample solutions were prepared by mixing DNA duplex (5 μM) and compounds **2**, **3**, **4** (20 μM) in 10 mM sodium phosphate buffer (aq., pH 7.0) and 100 mM NaCl. Thermal denaturation profiles were recorded on a SHIMADZU UV-2700 UV–vis spectrometer equipped with a SHIMADZU TMSPC-8 temperature controller. The absorbance of the samples was monitored at 260 nm from 2 °C to 80 °C with heating rate of 1 °C/min. Melting profiles ranged between 2 °C to 60 °C are given in Figure 5 in main text. Samples at the photostationary state at 365 nm (PSS^{365nm}) and 460 nm (PSS^{460nm}) light were prepared by photoirradiation with a light source, ZUV-C20H (365 nm, for 20 sec) and UHP-Black-LED-460 (460 nm, for 10 min) at a distance of 10 cm, respectively. Non-irradiated control samples contain compounds under thermally adapted states that were prepared by incubation at 60 ˚C for 1 h under dark condition. In the repeated irradiation experiments (Figure 5D in main text), the samples were not subjected to the thermal treatment. The T_m values were determined as the temperature crossing the melting curve and the median of two straight lines drawn for the single and duplex region in the melting curve.

4. SPR Analysis

Surface plasmon resonance (SPR) assay was performed using Biacore T200 platform (GE Healthcare, Life Science). Immobilization of oligonucleotides on Series S sensor chip SA surface was carried out using streptavidine-biotin coupling in HBS-EP+ buffer (10 mM pH 7.4 HEPES, 150 mM NaCl, 3 mM EDTA, 0.005% surfactant P20). 5'-Biotinylated oligonucleotides (5'-biotin-CTAAC$\underline{N_1}$GAATGTTTTCATTC$\underline{N_2}$GTTAG-3'; for GG mismatch $\underline{N_1}$ = $\underline{N_2}$ = G, for CC mismatch $\underline{N_1}$ = $\underline{N_2}$ = C, and for full match sequence $\underline{N_1}$ = C and $\underline{N_2}$ = G) were purchased from Eurofins genomics. Concentration of the 5'-biotinylated oligonucleotides were adjusted to be 0.6 μM in 10 mM HEPES-500 mM NaCl, which were injected onto the chip. The amounts of immobilization were 912.1, 924.6, and 922.8 response unit (RU) for GG mismatch, CC mismatch, fullmatch DNA, respectively. Blank immobilization was performed in the flow cell 1 to permit reference subtraction. Each compound was dissolved in HBS-EP+ buffer 5% DMSO and was irradiated with 365 nm light for 20 sec. The samples were injected onto the chip for 60 sec (contact time) at a flow rate of 30 μL/min, followed by injection of running buffer (180 s) as a dissociation phase. All sensorgrams were corrected by reference subtraction of blank flow cell response.

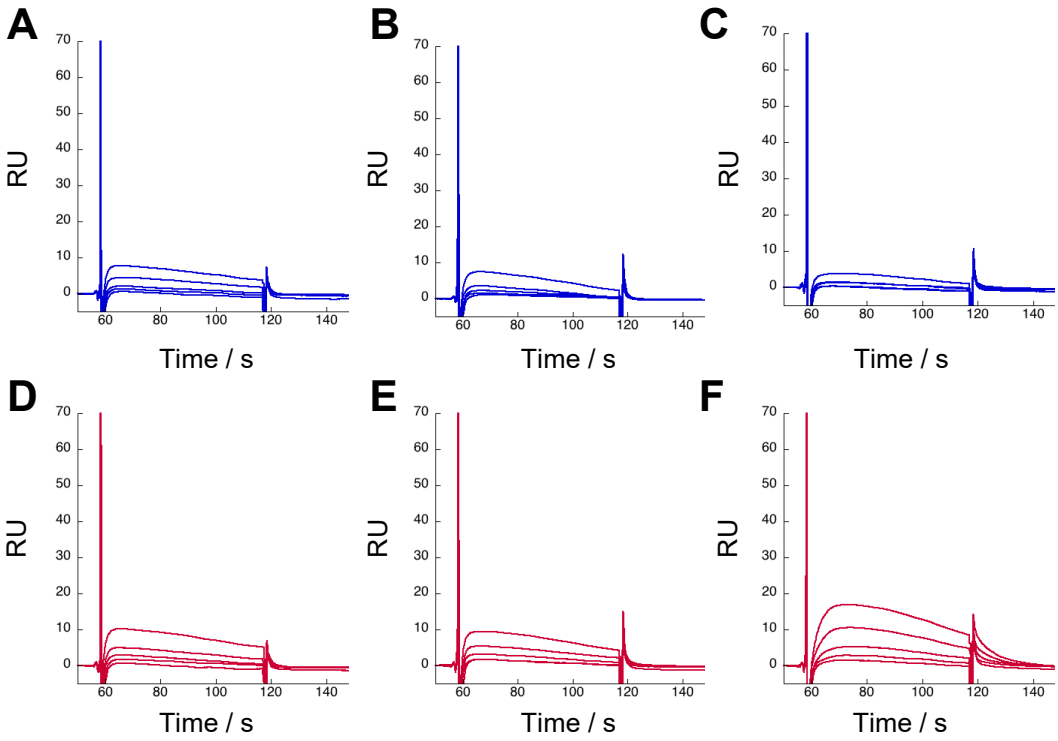

Figure S25. SPR analysis of the binding of ligands **2** (A, D), **3** (B, E), and **4** (C, F) to hairpin dsDNA containing a C$\underline{C}$G/C$\underline{C}$G site. Either ligands at thermal equilibrium (A, B, C) or ligands after irradiation at 365 nm (D, E, F) were injected to surface immobilized with the dsDNA containing a CC mismatch. Ligands at a series of concentrations (0.031, 0.063, 0.13, 0.25, 0.5 μM) were injected during association steps (from 57 to 117 s) followed by dissociation step where running buffer was injected.

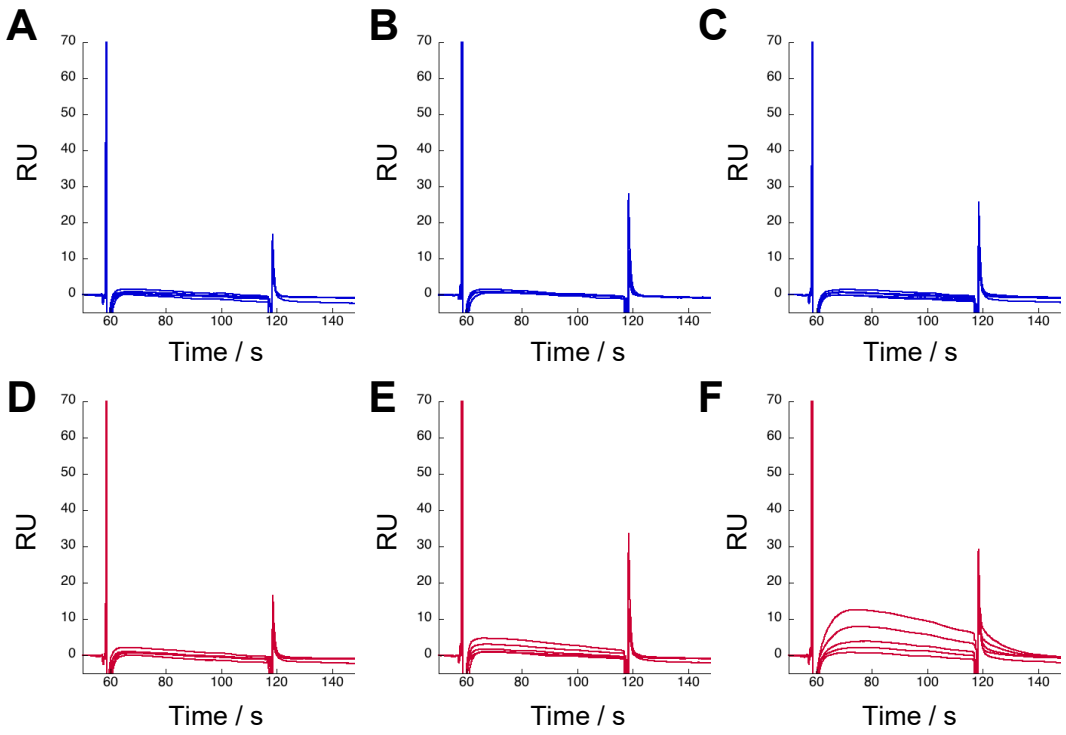

Figure S26. SPR analysis of the binding of ligands **2** (A, D), **3** (B, E), and **4** (C, F) to hairpin dsDNA containing a C<u>C</u>G/C<u>G</u>G site. Either ligands at thermal equilibrium (A, B, C) or ligands after irradiation at 365 nm (D, E, F) were injected to surface immobilized with the fullmatch dsDNA. Ligands at a series of concentrations (0.031, 0.063, 0.13, 0.25, 0.5 μM) were injected during association steps (from 57 to 117 s) followed by dissociation step where running buffer was injected.

5. CD Spectroscopy

Circular dichroism (CD) spectra were recorded on JASCO J815 CD spectrometer (scan-rate 20 nm/min). For a standard experiment, a fluorescence quartz cuvette (width = 1.0 cm) was equipped with 2 mL sample volume and studied at 25 °C. Irradiation was performed outside of the spectrometer with a suitable light source in a distance of *ca*. 1 cm. For irradiation, a 365 nm hand-held lamp (Spectroline ENB-280C), or a Sahlmann cooled 3 x Roithner SMB-1N 430h (426 nm, FWHM = 16 nm, power output = 600 mW), or a Sahlmann cooled 3 x Nichia NCSB219B-V1 (464 nm, FWHM = 28 nm, power output = 1000 mW), respectively, were used.

For binding studies, increasing amounts of MBL (1 mM stock solutions in water) were added to a fixed amount of an 11-mer dsDNA (5 µM in phosphate buffer) containing a d(CGG)/d(CGG) mismatch. The MBL stock solutions were thermally adapted and stored and handled in the dark. Cuvettes containing samples were handled in the dark or covered with aluminum foil until the measurement. To study the *Z* isomers, the respective cuvettes were irradiated after every ligand addition for 1 min in the case of **NCDA3** or 10 s in the case of compound **2** to **4**, respectively, with 365 nm light. Blue-light irradiation was conducted for 5 min for all samples.

Reversibility was investigated by irradiation of the same sample altering between UV and blue light to toggle between both PSSs using compound **3** an illustrative example.

5.1.NCDA3

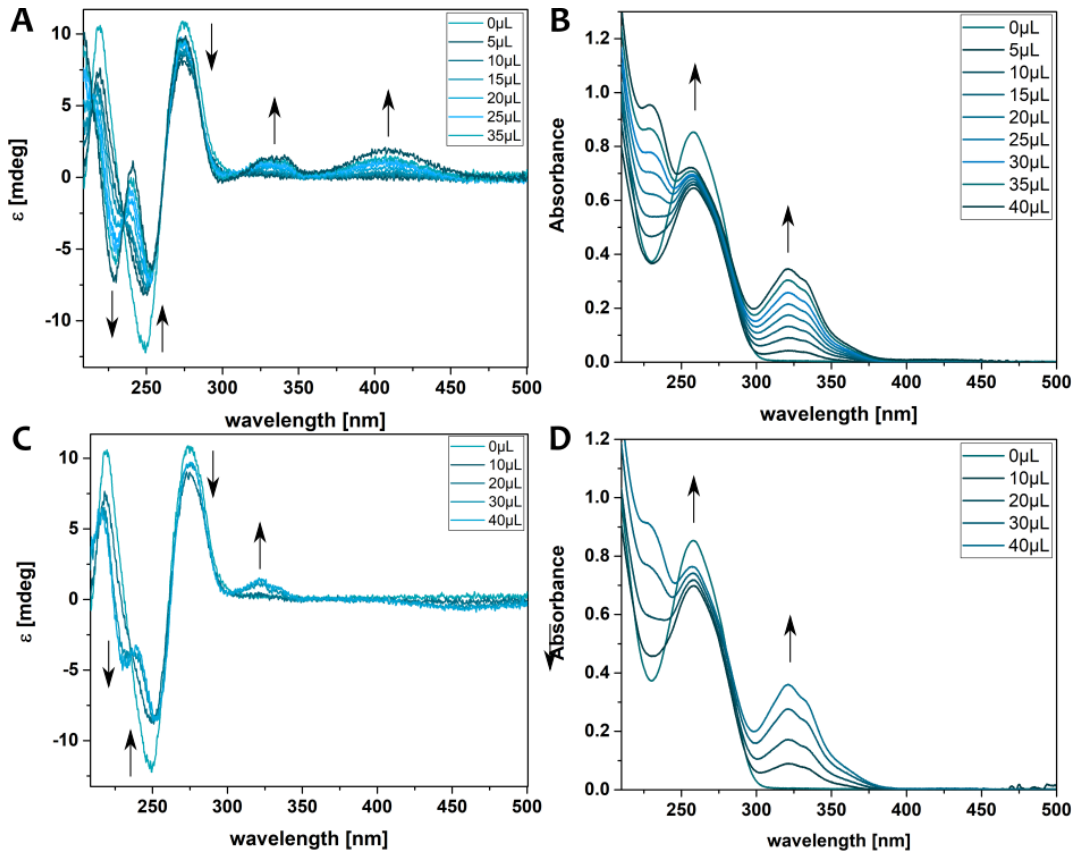

Figure S27. Titration of increasing amounts of MBL NCDA3 in phosphate buffer (aq., 0.01 M, 100 mM NaCl, pH = 7.0). **A**. CD spectra at the PSS^{365nm}. **B**. UV-Vis spectra at the PSS^{365nm}. **C**. CD spectra of the thermally adapted sample. **D**. UV-Vis spectra of the thermally adapted sample.

5.2.Compound **2**

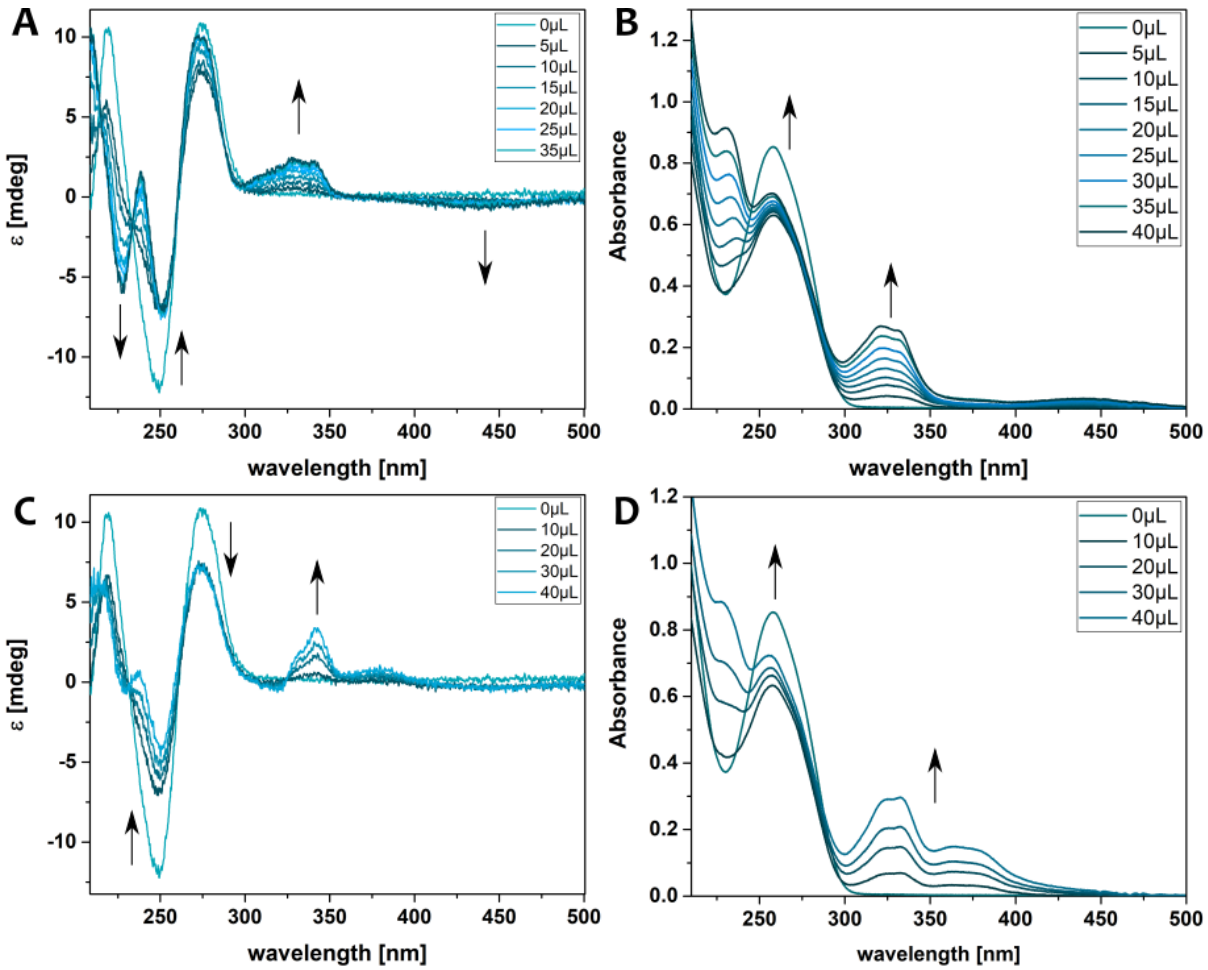

Figure S28. Titration of increasing amounts of MBL **2** in phosphate buffer (aq., 0.01 M, 100 mM NaCl, pH = 7.0). **A**. CD spectra at the PSS^{365nm}. **B**. UV-Vis spectra at the PSS^{365nm}. **C**. CD spectra of the thermally adapted sample. **D**. UV-Vis spectra of the thermally adapted sample.

5.3.Compound **3**

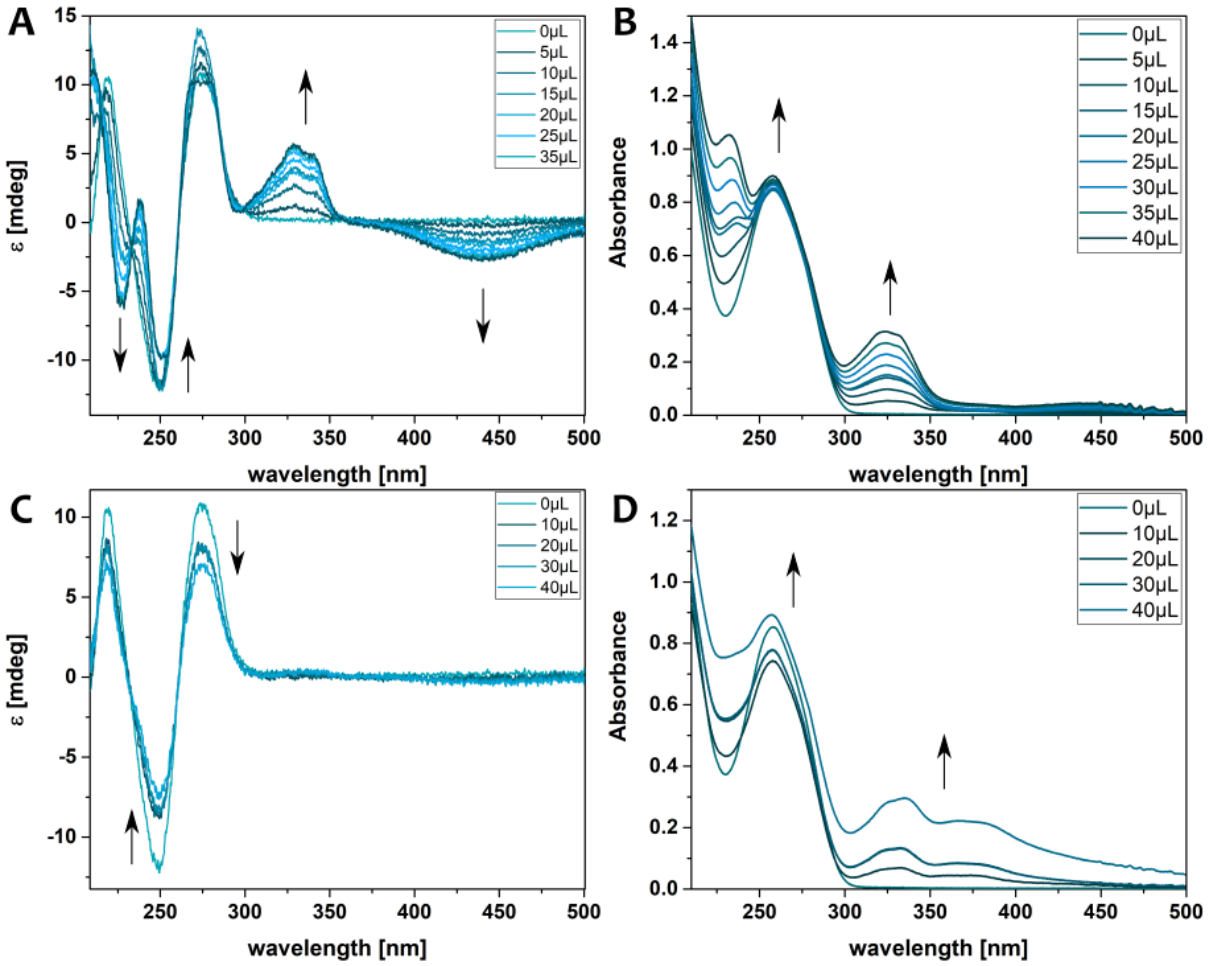

Figure S29. Titration of increasing amounts of MBL **3** in phosphate buffer (aq., 0.01 M, 100 mM NaCl, pH = 7.0). **A**. CD spectra at the PSS^{365nm}. **B**. UV-Vis spectra at the PSS^{365nm}. **C**. CD spectra of the thermally adapted sample. **D**. UV-Vis spectra of the thermally adapted sample.

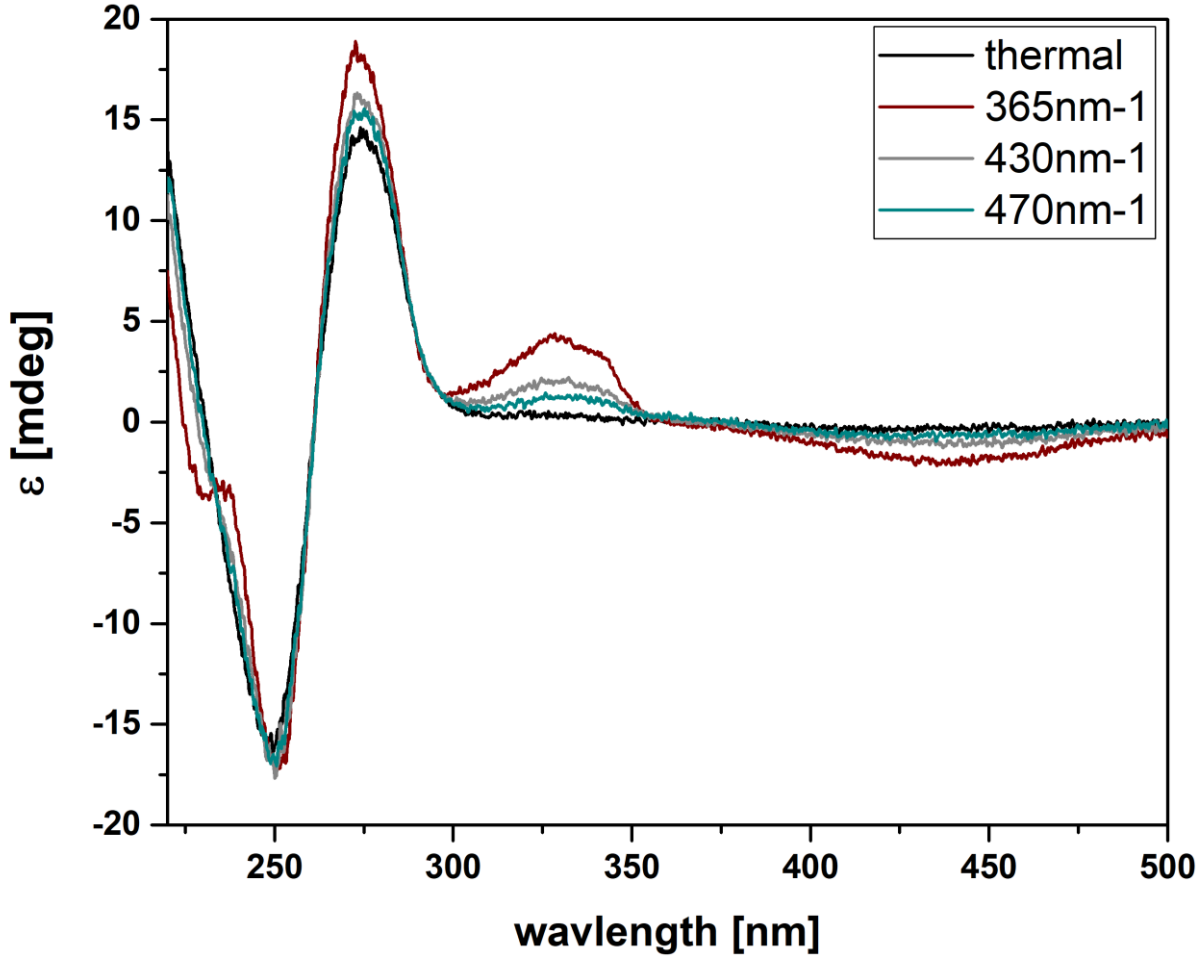

Figure S30. CD spectra of MBL **3** in phosphate buffer (aq., 0.01 M, 100 mM NaCl, pH = 7.0) at the thermal equilibrium (black), the PSS^{365nm} (red), the PSS^{430nm} (grey), and the PSS^{470nm} (cyan) containing varying amounts of *Z* isomer.

5.4.Compound **4**

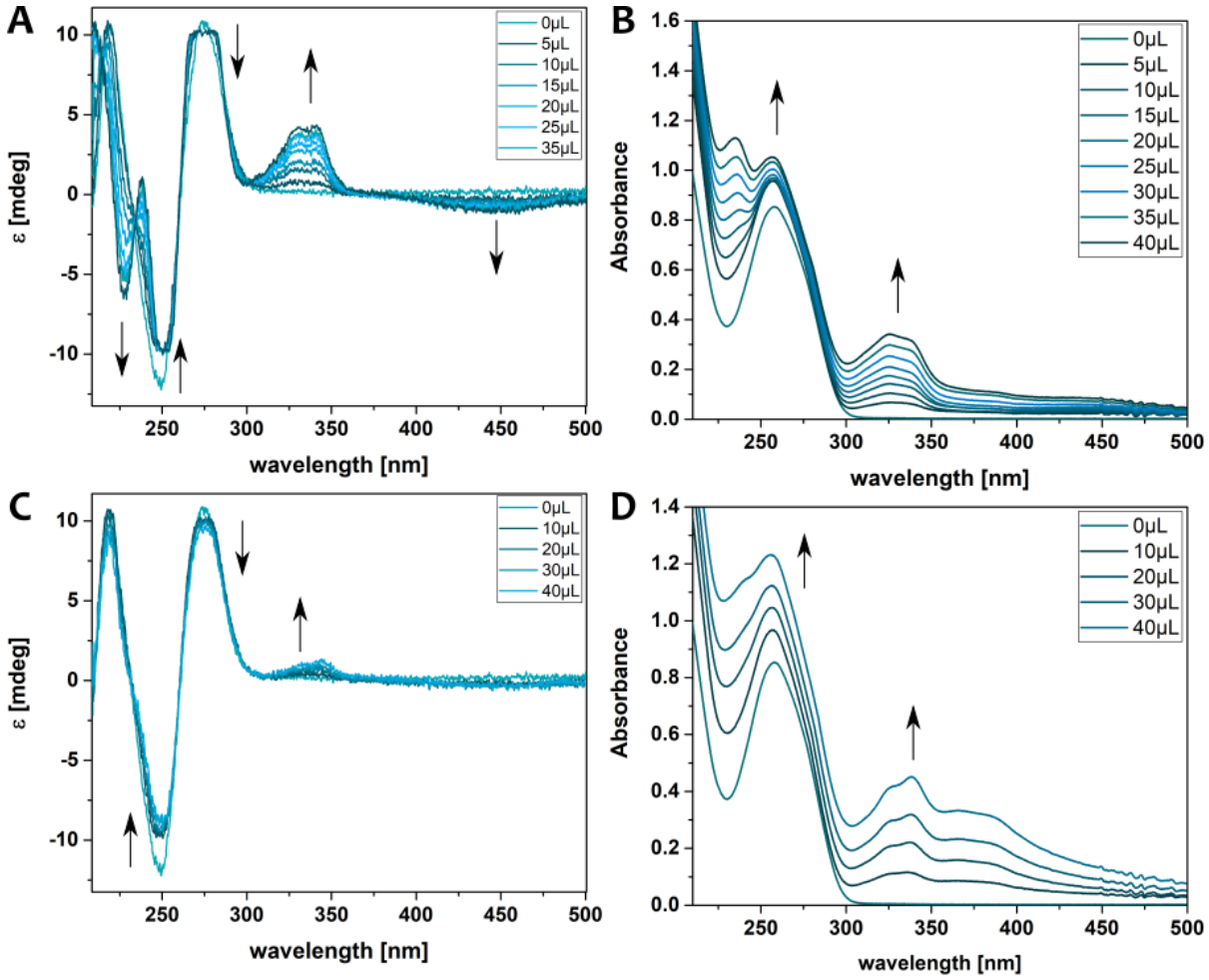

Figure S31. Titration of increasing amounts of MBL **4**. **A**. CD spectra at the PSS^{365nm}. **B**. UV-Vis spectra at the PSS^{365nm}. **C**. CD spectra of the thermally adapted sample. **D**. UV-Vis spectra of the thermally adapted sample.

5.5.Apparent K_D values

Apparent dissociation constant (K_D) was estimated by single set of identical binding sites model.[7] This is simplified binding model for the MBL–DNA interaction and only provide a rough estimation of K_D of each compound. CD titration data were fitted to following equation

$$\theta = \frac{1}{2}\frac{\theta_{max}}{n \cdot M_t}\left(\left(\frac{1}{K_A} + x + n \cdot M_t\right) - \sqrt{\left(\frac{1}{K_A} + x + n \cdot M_t\right)^2 - 4n \cdot M_t \cdot x}\right)$$

, where n is number of binding sites, K_A is binding constant, M_t is bulk concentration of DNA, x is bulk concentration of ligand, and θ_{max} is saturated value of CD. n is fixed to 2 according to reported binding stoichiometry of NCDA derivatives to CGG/CGG sequence.[4] Intensities at 341 nm in the induced CD band (Figures S28-31) are plotted against total (*Z* and *E*) concentration of each compound (Figure S32). Fitting to the equation provided qualitative KD values, 15.2, 0.7, and 23.6 μM for compound **2**, **3**, and **4**, respectively.

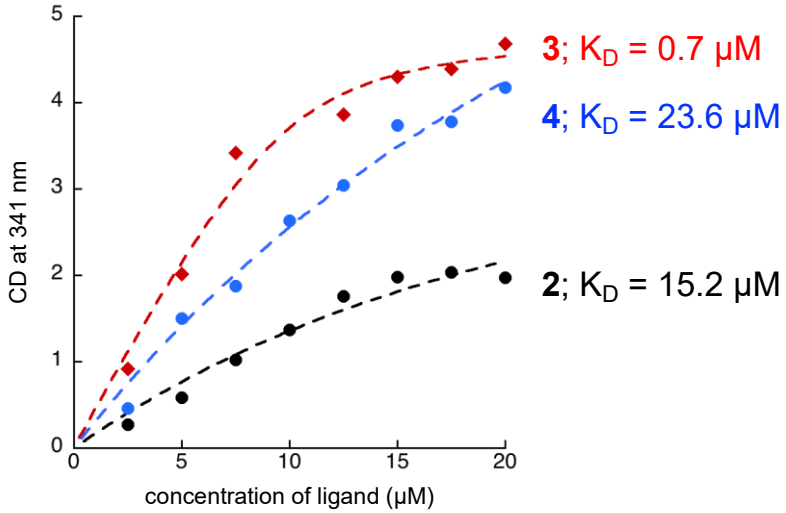

Figure S32. Qualitative fit of the titration studies to determine the apparent K_D value using a single set of identical sites model. Black filled circle, compound **2**; Red filled diamond, **3**; Blue filled circle, **4**.

6. Computational Data

6.1.Cartesian Coordinates of the optimized structures

The structures of both *E* and *Z* isomers of the model compounds as well as of the naphthyridine carbamate core were optimized at the ωB97X-D/def2-SVP level of theory in vacuum using the Gaussian 16, Version B.01 software package.[8] The cartesian coordinates, the energies and the thermochemical parameters of the structures are provided in the following section. All the compounds reported were confirmed to be minima after checking the absence of imaginary frequencies.

_E_-CH_2NHCH_3

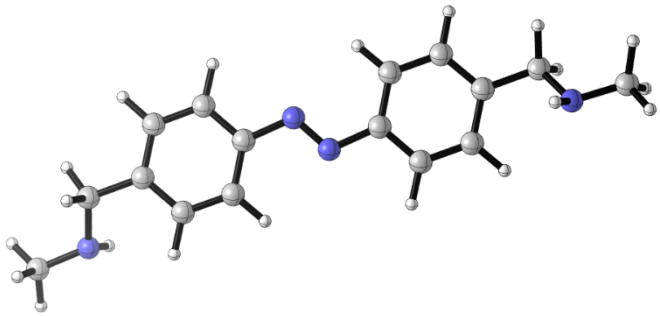

C	-3.75247293	-0.81118506	0.20516196
C	-4.56475076	0.33288953	0.2021894
C	-3.95704066	1.58930682	0.12713083
C	-2.57122325	1.70453697	0.06629909
C	-1.77072898	0.56017908	0.07114569
C	-2.37032908	-0.7052024	0.1393267
N	-0.37253603	0.77857412	0.00099492
N	0.32726422	-0.24707671	-0.00418046
C	1.72549113	-0.02931276	-0.0733499
C	2.52680269	-1.17352219	-0.07786576
C	3.91249923	-1.06220401	-0.14323548
C	4.51967545	0.19584373	-0.20247665
C	3.70714208	1.33898597	-0.1910698
C	2.32432713	1.23655601	-0.13108643
C	-6.06724418	0.20749535	0.3111752
C	6.02218585	0.3237824	-0.31018685
N	-6.57208356	-0.97881189	-0.34143105
C	-7.9967954	-1.1706319	-0.20198325
N	6.71988938	-0.75558723	0.34977001
C	8.15608956	-0.7097104	0.20330017
H	-4.23377301	-1.79001815	0.25261554
H	-4.57641413	2.49019493	0.11309646
H	-2.08276704	2.67900741	0.00678978
H	-1.73073212	-1.58847763	0.14038802
H	2.03688068	-2.14807787	-0.0301028

H	4.54687734	-1.95037842	-0.14339183
H	4.1723008	2.3282593	-0.22644193
H	1.68584433	2.12043727	-0.12057642
H	-6.33780324	0.14323594	1.38188814
H	-6.5363307	1.14705836	-0.05705965
H	6.30034109	0.29993106	-1.380593
H	6.32587225	1.33147785	0.05161492
H	-6.30397718	-0.97249306	-1.32271635
H	-8.31032483	-2.06864062	-0.75361488
H	-8.24942891	-1.33181813	0.85860856
H	-8.61104245	-0.31618472	-0.55953965
H	6.45943691	-0.78318706	1.3328076
H	8.61681037	-1.53749093	0.76145283
H	8.42722119	-0.83777698	-0.8572214
H	8.62150322	0.23841055	0.54907275

Energy= -839.8180282
Zero-point correction= 0.341198 (Hartree/Particle)
Thermal correction to Gibbs Free Energy= 0.290754
Sum of electronic and zero-point Energies= -839.476830
Sum of electronic and thermal Energies= -839.457693
Sum of electronic and thermal Enthalpies= -839.456749
Sum of electronic and thermal Free Energies= -839.527274

***Z*-CH_2NHCH_3**

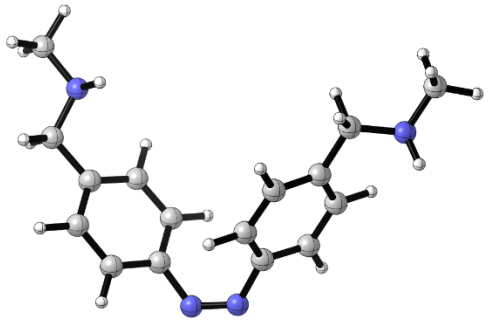

C	-2.34186416	0.13351592	-0.93151132
C	-3.34458839	0.15931815	0.04483123
C	-3.44884197	-0.92320358	0.92394708
C	-2.58420673	-2.0092244	0.82737636
C	-1.55767134	-1.99958371	-0.11906316
C	-1.44883043	-0.92856139	-1.01283306
N	-0.73826723	-3.16652724	-0.20982183
N	0.49696352	-3.1208472	-0.25789697
C	1.23878295	-1.91355523	-0.07445672
C	2.25476437	-1.63607854	-0.99230019
C	3.051818	-0.50796077	-0.830154
C	2.88721581	0.33169031	0.27727325

C	1.90439671	0.00980202	1.21889021
C	1.07607085	-1.09428591	1.04700725
C	-4.3212797	1.31121544	0.11384387
C	3.74293132	1.56730348	0.44142508
N	5.0753412	1.38970498	-0.08895457
C	5.90313425	2.5713676	-0.02160407
N	-3.71711366	2.56773702	-0.26678178
C	-4.63157422	3.68563496	-0.27955786
H	-2.26432408	0.97507126	-1.62255218
H	-4.2291365	-0.92432643	1.69001382
H	-2.68234849	-2.8693776	1.49266474
H	-0.66555143	-0.93054593	-1.77263963
H	2.40113516	-2.31176036	-1.83749899
H	3.83625203	-0.27242619	-1.55196946
H	1.78079666	0.6367068	2.10625213
H	0.3086126	-1.32727323	1.78684198
H	-5.15426009	1.11327512	-0.58641131
H	-4.78380345	1.33311877	1.12586945
H	3.27034838	2.4008897	-0.11124683
H	3.73128348	1.87645349	1.51047117
H	5.52846633	0.60555554	0.37442397
H	6.90811196	2.34800184	-0.40776148
H	5.47548479	3.36318555	-0.65787621
H	6.01428904	2.99500072	0.99979735
H	-2.91938769	2.76169262	0.3339343
H	-4.09352248	4.60781088	-0.54256575
H	-5.40486238	3.52614762	-1.04841272
H	-5.15759425	3.85796089	0.68416802

Energy= -839.79752
Zero-point correction= 0.341123 (Hartree/Particle)
Thermal correction to Gibbs Free Energy= 0.291393
Sum of electronic and zero-point Energies= -839.456397
Sum of electronic and thermal Energies= -839.437457
Sum of electronic and thermal Enthalpies= -839.436513
Sum of electronic and thermal Free Energies= -839.506127

***E*-OCH$_3$**

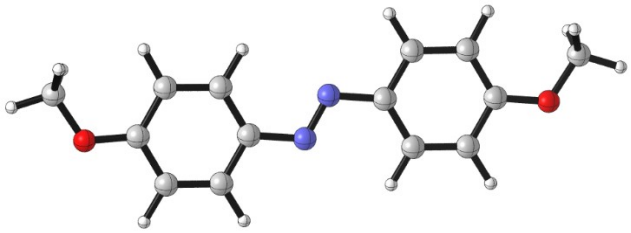

C	3.697662	1.293092	0.000087
C	4.525044	0.154485	0.00007
C	3.948188	-1.120399	-0.000037
C	2.55921	-1.242931	-0.000124
C	1.736693	-0.117741	-0.000109
C	2.322726	1.160786	0
N	0.34473	-0.357496	-0.000215
N	-0.373516	0.657129	-0.000203
C	-1.766449	0.419088	-0.000115
C	-2.591408	1.551725	-0.000063
C	-3.970328	1.422059	0.000015
C	-4.555409	0.146975	0.000044
C	-3.735401	-0.992363	-0.000011
C	-2.352062	-0.850941	-0.000088
O	5.850764	0.389739	0.000159
O	-5.901733	0.111447	0.000115
C	6.738266	-0.69545	0.000129
C	-6.556604	-1.128158	0.000196
H	4.174588	2.274752	0.000169
H	4.563942	-2.019563	-0.000053
H	2.087041	-2.227292	-0.000209
H	1.670768	2.034883	0.000008
H	-2.118519	2.535694	-0.000088
H	-4.626179	2.293885	0.000056
H	-4.166553	-1.993602	0.000002
H	-1.700978	-1.725882	-0.000135
H	7.750475	-0.27352	0.000195
H	6.61407	-1.325401	0.898093
H	6.614141	-1.325292	-0.897921
H	-7.632248	-0.914502	0.000287
H	-6.311104	-1.721235	-0.897843
H	-6.310945	-1.721203	0.898212

Energy= -800.9583381
Zero-point correction= 0.259059 (Hartree/Particle)
Thermal correction to Gibbs Free Energy= 0.214186
Sum of electronic and zero-point Energies= -800.699279
Sum of electronic and thermal Energies= -800.683501
Sum of electronic and thermal Enthalpies= -800.682557
Sum of electronic and thermal Free Energies= -800.744152

***Z*-OCH$_3$**

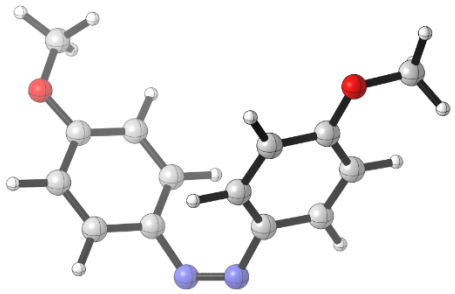

C	-2.01135269	0.42180974	-1.24787692
C	-3.06853079	0.67639996	-0.35938967
C	-3.27362749	-0.18074152	0.72715745
C	-2.42700755	-1.27371139	0.91329934
C	-1.34497456	-1.4948093	0.06460794
C	-1.15508278	-0.6445914	-1.03642717
N	-0.57071246	-2.67376746	0.29007323
N	0.66677255	-2.69491232	0.24666677
C	1.46864067	-1.51929902	0.13157137
C	2.54177807	-1.56115648	-0.76774502
C	3.40126698	-0.48149268	-0.88713594
C	3.23908852	0.64591401	-0.06764331
C	2.20165898	0.66805368	0.87229003
C	1.31985334	-0.40752739	0.96169939
O	-3.83396913	1.7506371	-0.63942914
O	4.12944636	1.64306643	-0.24390219
C	-4.91923725	2.05022442	0.19484695
C	4.02691512	2.79703519	0.54440836
H	-1.88296196	1.08663892	-2.10347417
H	-4.09747643	-0.02362763	1.42322433
H	-2.59761374	-1.96927205	1.73748788
H	-0.33407039	-0.82617153	-1.73170425
H	2.68097505	-2.45491703	-1.37922787
H	4.22779101	-0.49034218	-1.59937468
H	2.06456587	1.51806372	1.54050479
H	0.50940049	-0.37679943	1.69166654
H	-5.39274263	2.95026557	-0.21554537
H	-5.66141619	1.23302225	0.2113636
H	-4.59558155	2.25830582	1.22985186
H	4.83582901	3.46673872	0.22835104
H	3.06064887	3.3102113	0.39599728
H	4.15008289	2.57236683	1.61837289

Energy= -800.9355395
Zero-point correction= 0.258698 (Hartree/Particle)
Thermal correction to Gibbs Free Energy= 0.214176
Sum of electronic and zero-point Energies= -800.676841
Sum of electronic and thermal Energies= -800.661195
Sum of electronic and thermal Enthalpies= -800.660251
Sum of electronic and thermal Free Energies= -800.721364

Naphthyridine Carbamate Core

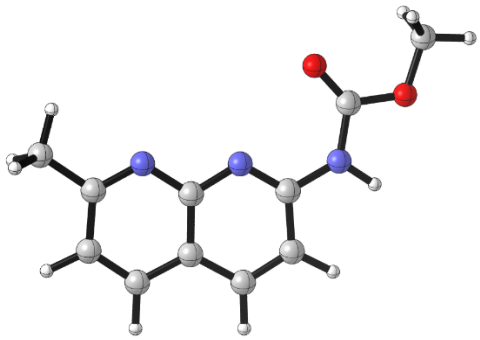

C	5.27217528	-1.01452077	-0.00018759
O	4.30949858	0.02313602	-0.00002403
C	3.0195378	-0.38030549	0.00016057
N	2.23631189	0.76039081	0.00010496
O	2.66866746	-1.52250984	0.00006732
C	0.84849262	0.87293522	0.00007722
N	0.10332997	-0.19538204	0.0000552
C	-1.24454315	-0.05632013	-0.00003143
C	-1.86953601	1.22220477	-0.00003777
C	-1.03121365	2.36789435	-0.00002722
C	0.32386409	2.20717795	0.00001883
N	-1.96863009	-1.20116871	0.00002114
C	-3.27979169	-1.13628392	0.00001082
C	-3.99082887	0.10018396	-0.00005923
C	-3.28403178	1.27300414	-0.00006754
C	-4.04550283	-2.43124569	0.00000438
H	6.25159826	-0.52280984	-0.0004101
H	5.16835686	-1.64897161	0.8920973
H	5.16798439	-1.64904373	-0.89237674
H	2.76330761	1.62350951	0.00008555
H	-1.47641127	3.36607794	-0.00005124
H	0.99605403	3.06776172	0.0000216
H	-5.08267027	0.09766368	-0.00009655
H	-3.79137369	2.24159055	-0.00009732
H	-3.34299337	-3.2728714	-0.00016167
H	-4.69385433	-2.50164102	0.88728211
H	-4.69413977	-2.50150211	-0.88707476

Energy= -739.7516139
Zero-point correction= 0.213184 (Hartree/Particle)
Thermal correction to Gibbs Free Energy= 0.169885
Sum of electronic and zero-point Energies= -739.538430
Sum of electronic and thermal Energies= -739.524249
Sum of electronic and thermal Enthalpies= -739.523305
Sum of electronic and thermal Free Energies= -739.581729

6.2.TD-DFT Spectra

Using the optimized geometries, we simulated the UV-Vis spectra of the different components using TD-DFT at the PBE0/6-311+G(2d,p) level of theory using a conductor-like polarizable continuum model (C-PCM, ε= 78.4 for water).[9] Single point calculations up to the first 25 singlet states were performed to describe the UV-Vis absorption spectra. The five lowest transitions are reported including the energy (in eV), the associated wavelength (in nm), and its oscillator strength. The numbers of the orbitals involved in the transition (with general formula occupied → unoccupied) and the associated (largest) coefficient in the CI expansion is depicted.

The spectra were processed using GaussView 6.0.16 and OriginPro 2016.

***E*-CH_2NHCH_3**

Excited State 1: Singlet-A 2.6805 eV 462.55 nm f=0.0001
69 → 73 0.67532
71 → 73 -0.15880

Excited State 2: Singlet-A 3.2908 eV 376.76 nm f=0.5364
72 → 73 0.70115

Excited State 3: Singlet-A 3.4106 eV 363.52 nm f=0.0002
69 → 73 0.15827
71 → 73 0.68468

Excited State 4: Singlet-A 3.6290 eV 341.65 nm f=0.6110
70 → 73 0.69703

Excited State 5: Singlet-A 4.1720 eV 297.18 nm f=0.0475
68 → 73 0.67891
70 → 74 -0.11821
72 → 74 -0.12284

***Z*-CH_2NHCH_3**

Excited State 1: Singlet-A 2.7042 eV 458.48 nm f=0.0662
66 → 73 0.19131
68 → 73 0.12373
70 → 73 0.30682

72 → 73 0.58662

Excited State 2: Singlet-A 3.6784 eV 337.06 nm f=0.0434
66 → 73 0.11137
70 → 73 0.36357
71 → 73 0.50956
72 → 73 -0.28215

Excited State 3: Singlet-A 3.7229 eV 333.03 nm f=0.0152
70 → 73 -0.44090
71 → 73 0.47626
72 → 73 0.24229

Excited State 4: Singlet-A 4.0897 eV 303.16 nm f=0.0994
66 → 73 0.25702
68 → 73 0.58056
70 → 73 -0.24659

Excited State 5: Singlet-A 4.1749 eV 296.97 nm f=0.0313
69 → 73 0.67619

***E*-OCH$_3$**

Excited State 1: Singlet-A 2.8024 eV 442.42 nm f=0.0000
63 → 65 0.70180

Excited State 2: Singlet-A 3.2433 eV 382.27 nm f=1.1184
64 → 65 0.70524

Excited State 3: Singlet-A 4.2703 eV 290.34 nm f=0.0073
60 → 65 -0.22969
61 → 65 -0.10470
62 → 65 0.63658
64 → 66 0.10882

Excited State 4: Singlet-A 4.3671 eV 283.91 nm f=0.0005
60 → 65 -0.13800
61 → 65 0.60058
64 → 66 -0.28536
64 → 67 0.13028

Excited State 5: Singlet-A 4.4040 eV 281.52 nm f=0.0001
60 → 65 0.55876
62 → 65 0.25828
64 → 66 -0.11745
64 → 67 -0.27078

***Z*-OCH$_3$**

Excited State 1: Singlet-A 2.6491 eV 468.02 nm f=0.0971
62 → 65 0.25273
64 → 65 0.64890

Excited State	2:	Singlet-A	3.8493 eV	322.10 nm	f=0.1955
61 → 65	0.11326				
62 → 65	0.62454				
63 → 65	0.10680				
64 → 65	-0.26746				
Excited State	3:	Singlet-A	3.9322 eV	315.30 nm	f=0.0860
63 → 65	0.67553				
Excited State	4:	Singlet-A	4.2783 eV	289.80 nm	f=0.0207
61 → 65	-0.36036				
64 → 66	0.59123				
Excited State	5:	Singlet-A	4.5252 eV	273.99 nm	f=0.0039
60 → 65	0.46952				
63 → 66	0.13681				
64 → 67	0.49260				

Naphthyridine Carbamate Core

Excited State	1:	Singlet-A	4.2078 eV	294.65 nm	f=0.3939
55 → 59	-0.19310				
57 → 58	0.67665				
Excited State	2:	Singlet-A	4.3471 eV	285.21 nm	f=0.0001
56 → 58	0.69848				
Excited State	3:	Singlet-A	4.8696 eV	254.61 nm	f=0.0038
55 → 58	0.58229				
57 → 59	0.38622				
Excited State	4:	Singlet-A	5.0049 eV	247.73 nm	f=0.0023
54 → 58	0.64164				
56 → 59	-0.23675				
56 → 60	0.13738				
Excited State	5:	Singlet-A	5.2127 eV	237.85 nm	f=0.0007
54 → 58	0.21497				
56 → 59	0.65542				
56 → 60	0.12474				

6.3.Conformational Search and Molecular Dynamic Simulations

The calculations and analysis were performed either on a HP EliteDesk, with an Intel Core i7-6700 processor with four cores and an NVIDIA GeForce GTX 1060 3GB graphics card (System preparation and Conformational search), or on the Peregrine cluster at the University of Groningen (Molecular Dynamics). The system preparation and the conformational search were carried out with Maestro (ver 12.4, Schrödinger Release 2020-2: Maestro, Schrödinger, LLC, New York, NY, 2020), using the OPLS3e force field.[10] Molecular Dynamics (MD) simulations were performed using GROMACS 2018.4.[11] The dihedral measurements were performed with KNIME (ver 4.1.1, KNIME AG, Zurich, Switzerland), using Schrödinger nodes and a custom Python script (based on the measure_by_smarts.py script) provided by Schrödinger. All the plots were generated with OriginPro 2019.

6.3.1. Preparation of the models

The model of the glue-DNA complex was built by modifying a similar structure that was previously released (PDB ID: 1X26).[12] Five structures were chosen out of the 30 NMR conformers using Clustering of conformers in Maestro (Hierarchical sampling, on atomic RMSD for heavy atoms, RMSD in place, linkage method: Ward, output: 5 clusters). The structure which was the closest to the centroid of each cluster was selected, i.e. conformers 3, 11, 13, 23 and 28. The molecular glues of these five complexes were manually modified to compound *Z*-**2**, *Z*-**3**, and *Z*-**4**, then prepared with the Protein Preparation Wizard (restrained minimization to 0.8 Å RMSD) and finally minimized with MacroModel (method: TNCG, 50000 max iterations). Concurrently, the molecular glues of the 5 selected complexes (conformers 3, 11, 13, 23 and 28) were deleted to produce 5 complexes without any photoswitchable glue. In total, this workflow generated 15 complexes with photoswitchable glues (*Z*-**2**, *Z*-**3** and *Z*-**4**) and 5 complexes with no photoswitchable glue.

6.3.2. Conformational search

The conformational search on the 15 complexes with photoswitchable glues (*Z*-**2**, *Z*-**3** and *Z*-**4**) was carried out with MacroModel (OPLS3e force field). The DNA atoms were kept frozen and a distance constraint (1000 kJ/mol) was applied between the DNA and the glue atoms involved in a hydrogen bond (enhanced sampling, method: TNCG, 50000 max iterations, convergence threshold 0.05, 62.8 kJ/mol window, redundant conformers with max atom deviation of 0.5 Å are eliminated). Finally, the complexes were minimized with MacroModel with no constraints. The potential energies calculated in this last step were visualized through violin plots (Figure S33). The complexes with *Z*-**4** consistently resulted in higher energies, thus suggesting that complexes with *Z*-**2** and *Z*-**3** would be energetically more favorable.

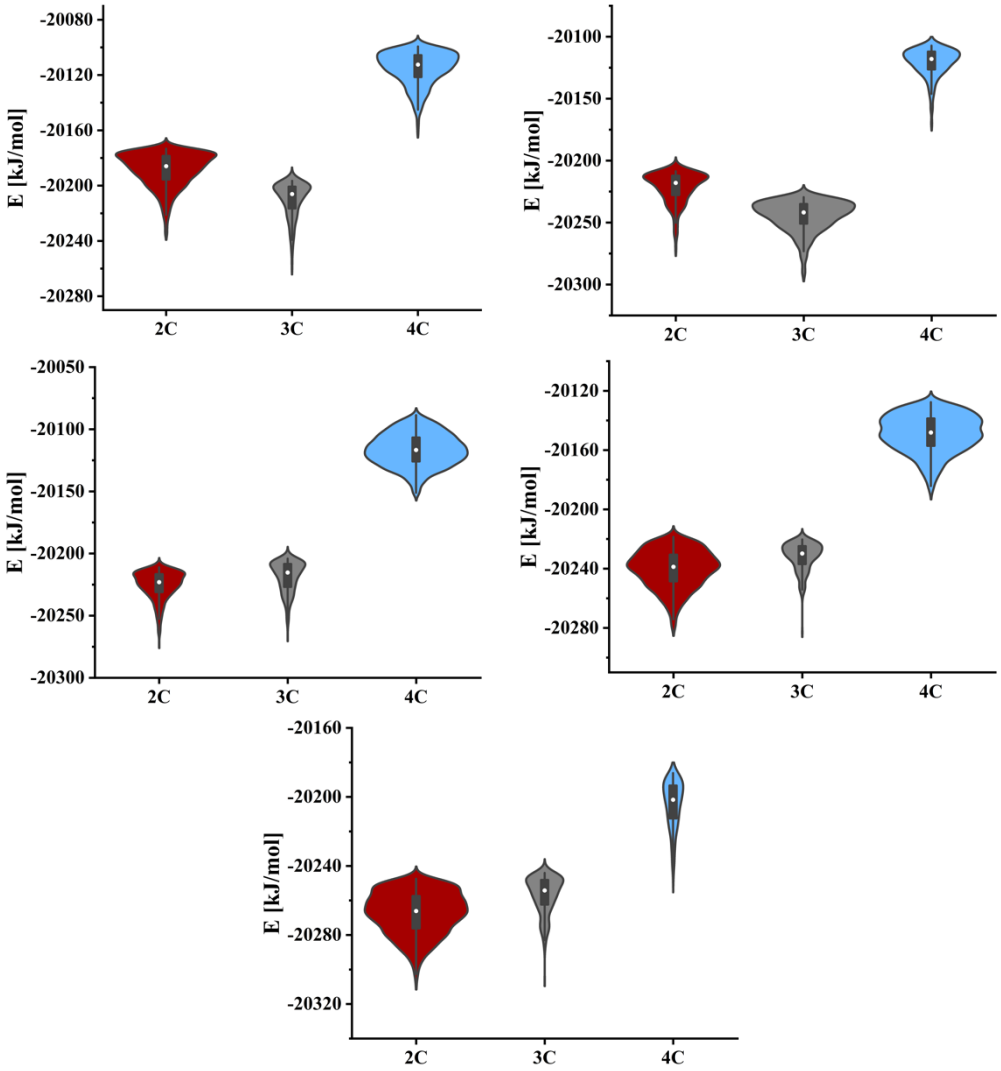

Figure S33. Violin plots of the potential energy calculated with the conformational search. of the photoswitchable glue- DNA 2:1 complexes with *Z*-**2** (2C), *Z*-**3** (3C), and *Z*-**4** (4C). From left to right: conformer 3, 11, 13, 23 and 28.

6.3.3. Molecular dynamics (MD) simulations

All the models prepared in the first subsection (15 complexes with and 5 complexes without photoswitchable glue)were further studied with MD. The parameter files for the MD simulations were prepared using the tLeap module of Ambertools and the DNA.bsc1 force field for DNA. Glue parameters were obtained using the Antechamber module[13] and AM1-BCC charge methods. The dihedral parameters for the azobenzene moiety were adapted from a previous study.[14] The general outlook of the dihedral section of the .top files is as follows:

ai	aj	ak	al	funct	c0	c1	c2
c	N	N	c	9	0.0	31.5	1
c	N	N	c	9	180.0	60.0	2
N	N	c	c	1	180.0	16.0	2
N	N	c	c	1	180.0	0.0	2
c	c	N	N	1	180.0	16.0	2

c c N N 1 180.0 0.0 2

The starting structures were immersed in a pre-equilibrated cubic box of around 10000 TIP3P water molecules with 0.1 M NaCl, and sodium ions were added to maintain the electrical neutrality. The systems were minimized over 50000 steps of the steepest descent algorithm before MD simulations were performed. The minimized structures were used as a starting point for the MD simulations at increasing temperatures (300, 325, 350, 400 and 500 K). During the equilibration steps, the heavy atoms of the DNA-glue complex were kept fixed with a constraint of 1000 kcal/mol. In the first step, a constant volume simulation (NVT) was performed, during which the system was heated from 0 K to the target temperature over 100 ps. In the second step, an isothermal and isobaric simulation (NPT) was performed using the Berendsen algorithm for 100 ps. After the equilibration steps, the systems were further relaxed with 1 ns of unrestrained MD, using the Parrinello-Rahman algorithm for pressure coupling. Finally, 300 ns MD production trajectories were run without restraint, collecting frames at 100 ps intervals and using a 2 fs time step. Particle mesh Ewald (PME)[15] was used to treat the long-range electrostatic interactions. All bonds were constrained using the LINCS algorithm. Gmx rms was used to calculate the RMSD of the DNA heavy atoms after least square fitting to the DNA heavy atoms. The complexes with *Z*-**3** consistently showed a higher stability (RMSD < 1.5 Å) than the other complexes throughout 300 ns MD simulations at increasing temperatures (Figure S34-S38).

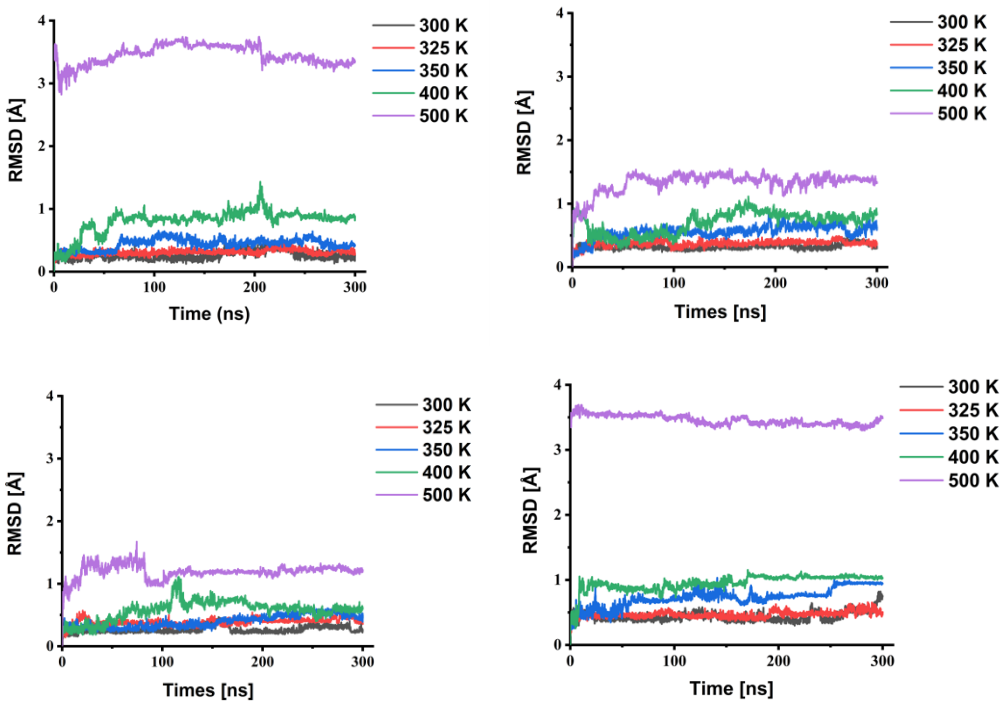

Figure S34. RMSD of DNA throughout the 300 ns MD simulation at increasing temperatures for conformer 3. From left to right: complexes with *Z*-**2**, *Z*-**3,** *Z*-**4**, and with no glue.

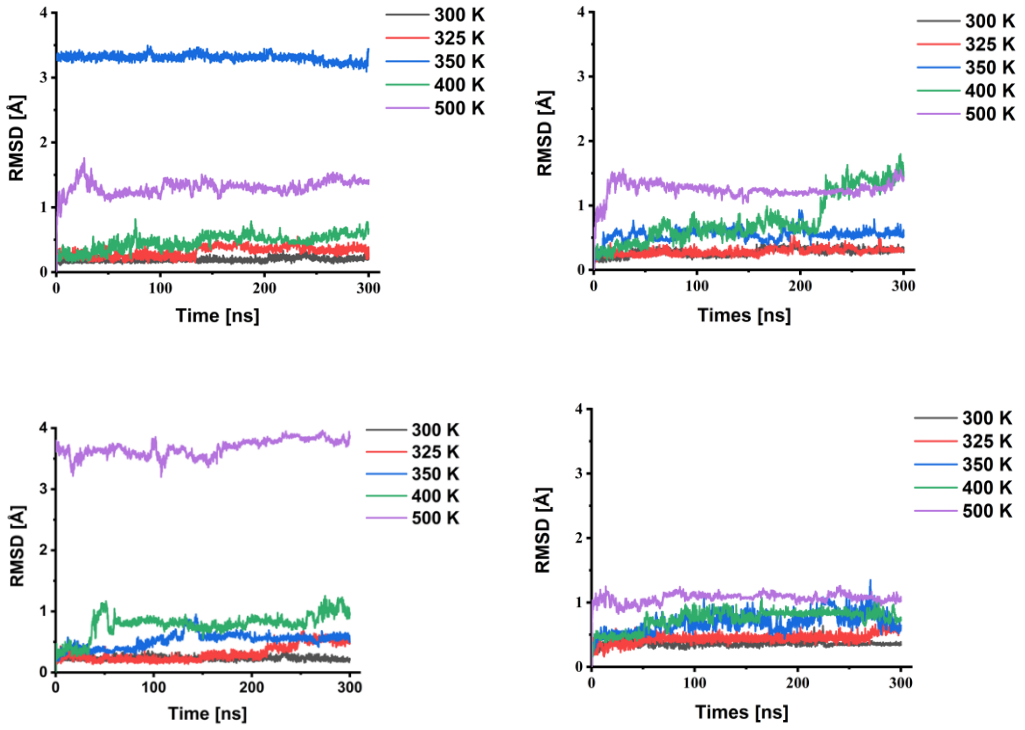

Figure S35. RMSD of DNA throughout the 300 ns MD simulation at increasing temperatures for conformer 11. From left to right: complexes with *Z*-**2**, *Z*-**3,** *Z*-**4**, and with no glue.

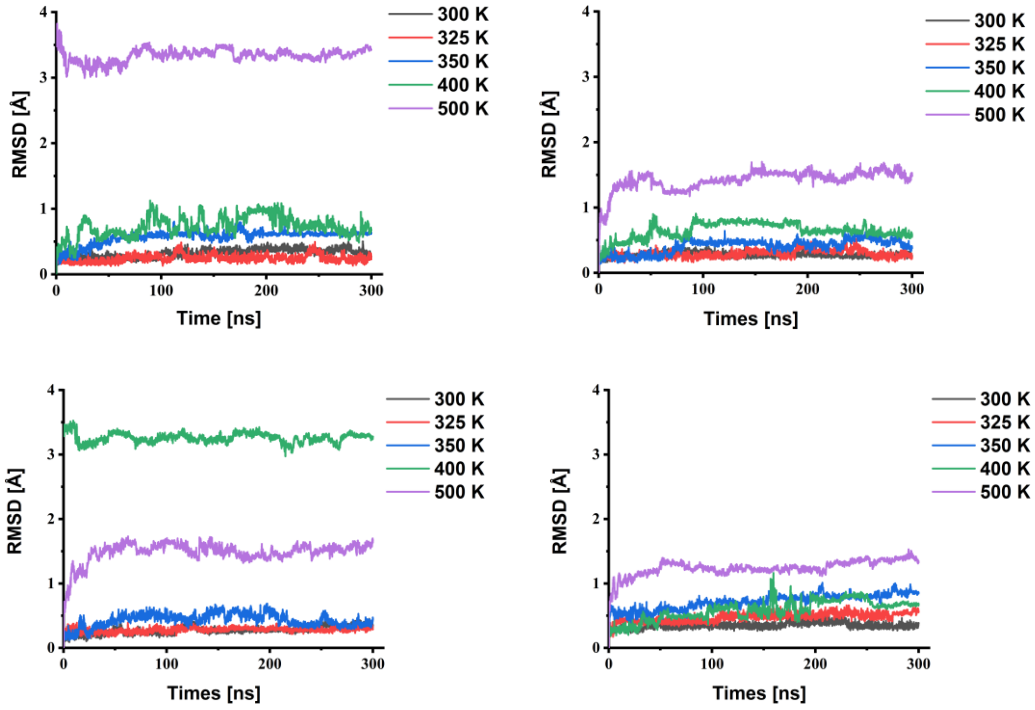

Figure S36. RMSD of DNA throughout the 300 ns MD simulation at increasing temperatures for conformer 13. From left to right: complexes with *Z*-**2**, *Z*-**3,** *Z*-**4**, and with no glue.

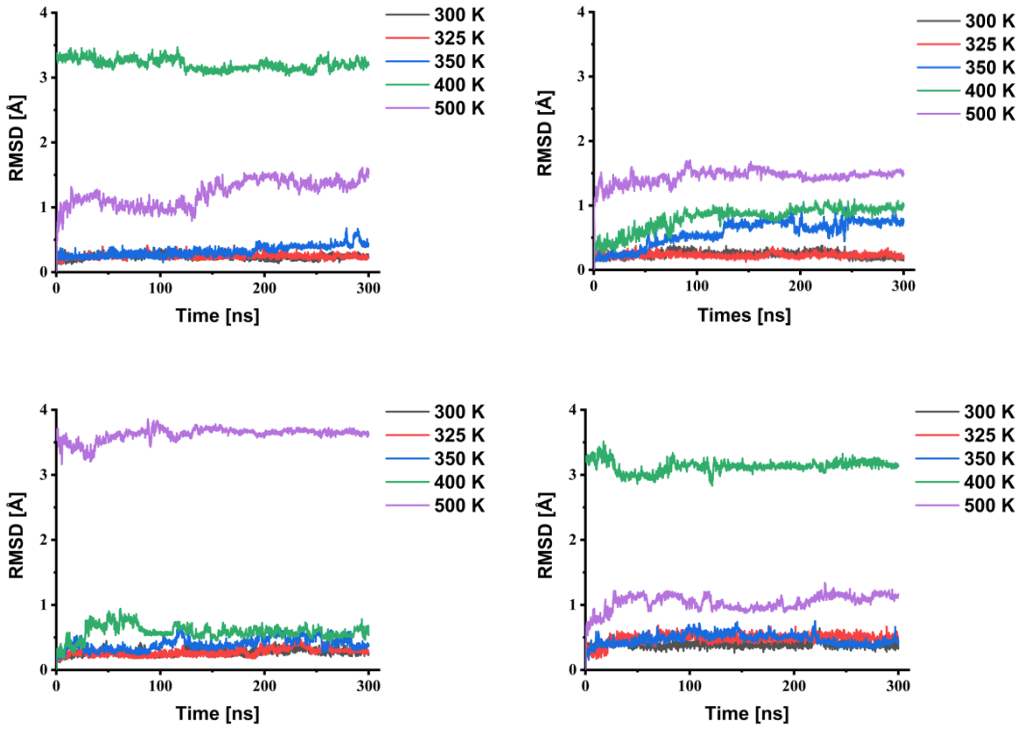

Figure S37. RMSD of DNA throughout the 300 ns MD simulation at increasing temperatures for conformer 23. From left to right: complexes with *Z*-**2**, *Z*-**3,** *Z*-**4**, and with no glue.

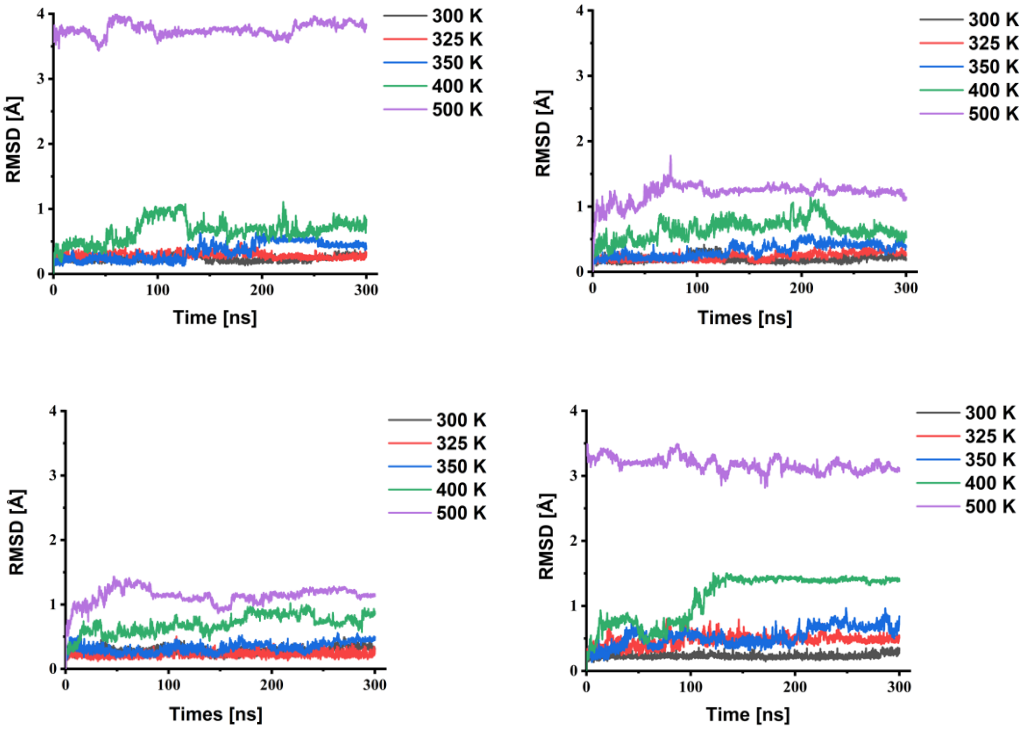

Figure S38. RMSD of DNA throughout the 300 ns MD simulation at increasing temperatures for conformer 28. From left to right: complexes with *Z*-**2**, *Z*-**3,** *Z*-**4**, and with no glue.

6.3.4. Analysis of (*M*)*Z* and (*P*)*Z* helical configurations

Gmx trjconv was used to extract 301 snapshots (every 1 ns) from the 300 ns MD runs at 300K. The structures without the explicit solvent shell were then optimized at the GFN-FF level, using the Born implicit solvent model for water. All the optimization were carried out with the xTB software package.[16]

The output structures were analyzed through KNIME to measure the ccNN dihedral angles with the measure_by_smarts.py script by Schrödinger. The helicity around the *cis*-azo double bond for each photoswitchable glue molecule was defined based on the ccNN/NNcc dihedral angle ϕ, as follows:

Helicity	**Φ (°)**
M	-90 < x < -10 v 90 < x < 170
P	10 < x < 90 v -170 < x < -90

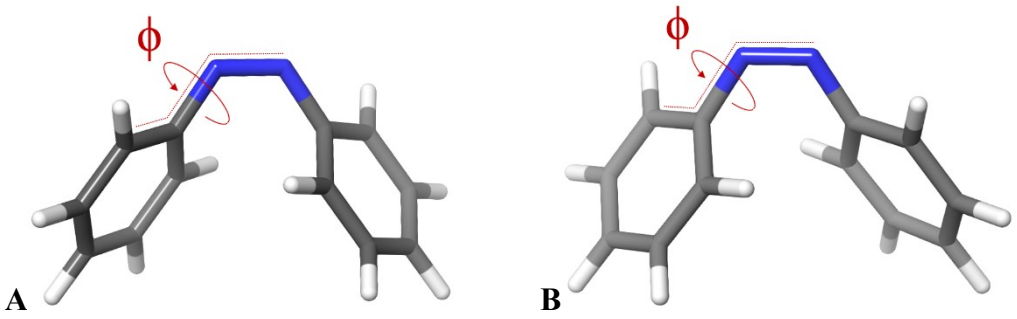

Figure S39. The dihedral angle used for the definition of the helicity. **A.** *(M)Z*-azobenzene. **B.** *(P)Z*-azobenzene.

The systems could adopt three different configurations: (*PP*)*Z*, a mixed (*PM/MP*)*Z*, and (*MM*)*Z*. Based on these three configurations, the energies obtained at the GFN-FF level were visualized through violin plots (Figure S40-44). The complexes showed a preference for (*PP*)*Z*, especially compared to the (*MM*)*Z* configuration.

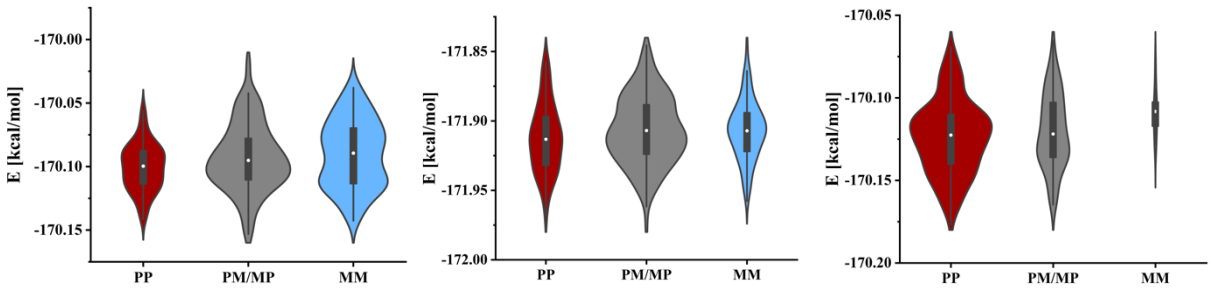

Figure S40. Conformer 3. Violin plots of the energy and distribution of two molecules of *Z*-**2** (left), *Z*-**3** (center) and *Z*-**4** (right) in a 2:1 complex to mismatched DNA adopting (*PP*)*Z*, (*PM/MP*)*Z*, and (*MM*)*Z*.

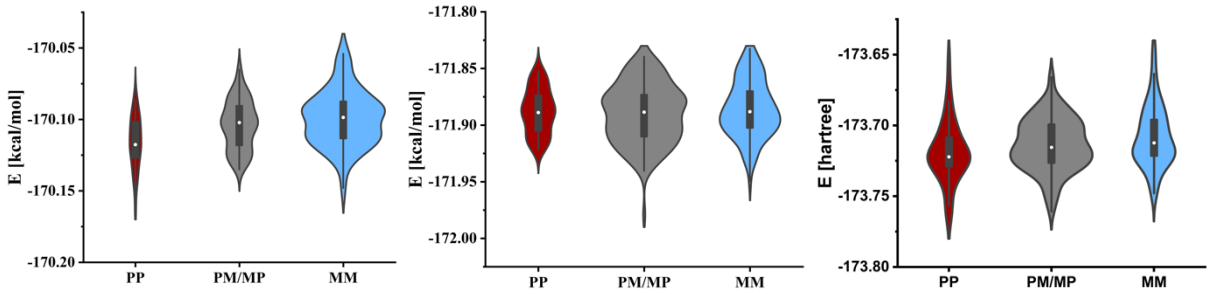

Figure S41. Conformer 11. Violin plots of the energy and distribution of two molecules of *Z*-**2** (left), *Z*-**3** (center) and *Z*-**4** (right) in a 2:1 complex to mismatched DNA adopting (*PP*)*Z*, (*PM/MP*)*Z*, and (*MM*)*Z*.

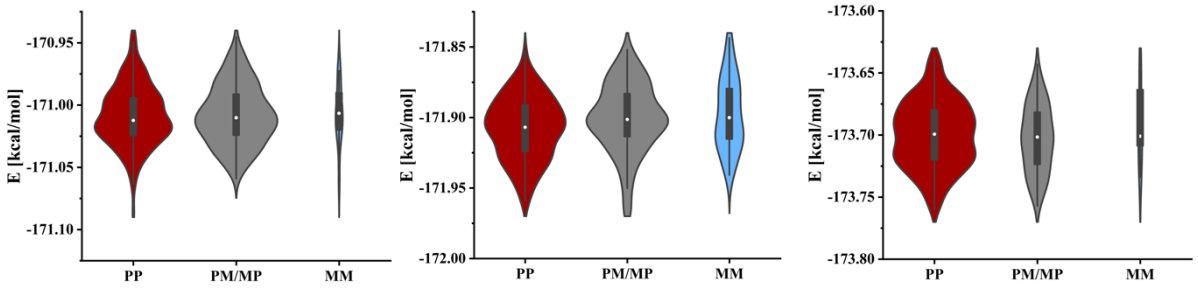

Figure S42. Conformer 13. Violin plots of the energy and distribution of two molecules of *Z*-**2** (left), *Z*-**3** (center) and *Z*-**4** (right) in a 2:1 complex to mismatched DNA adopting (*PP*)*Z*, (*PM/MP*)*Z*, and (*MM*)*Z*.

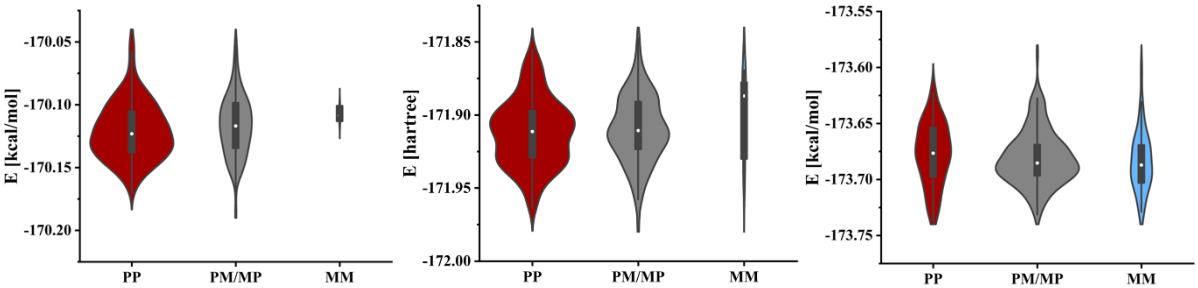

Figure S43. Conformer 23. Violin plots of the energy and distribution of two molecules of *Z*-**2** (left), *Z*-**3** (center) and *Z*-**4** (right) in a 2:1 complex to mismatched DNA adopting (*PP*)*Z*, (*PM/MP*)*Z*, and (*MM*)*Z*.

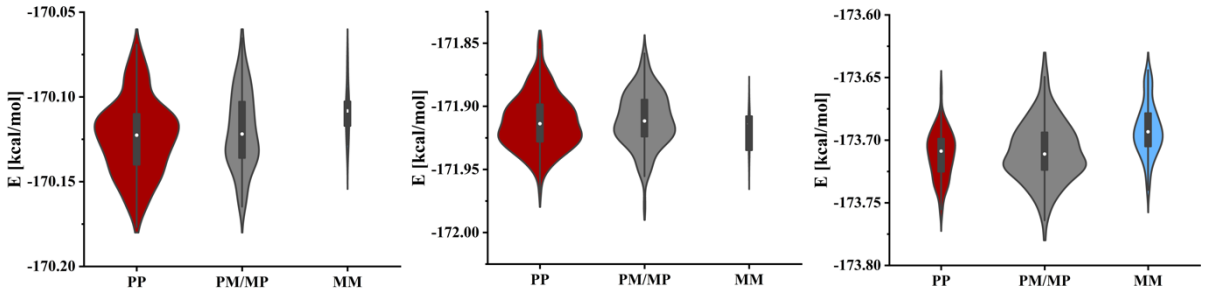

Figure S44. Conformer 28. Violin plots of the energy and distribution of two molecules of *Z*-**2** (left), *Z*-**3** (center) and *Z*-**4** (right) in a 2:1 complex to mismatched DNA adopting (*PP*)*Z*, (*PM/MP*)*Z*, and (*MM*)*Z*.

7. NMR-Data

Compound 6 (^{1}H NMR; 400 MHz, Chloroform-*d* : Methanol-*d4* 1:1)

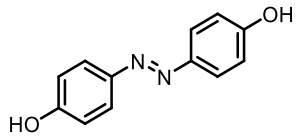

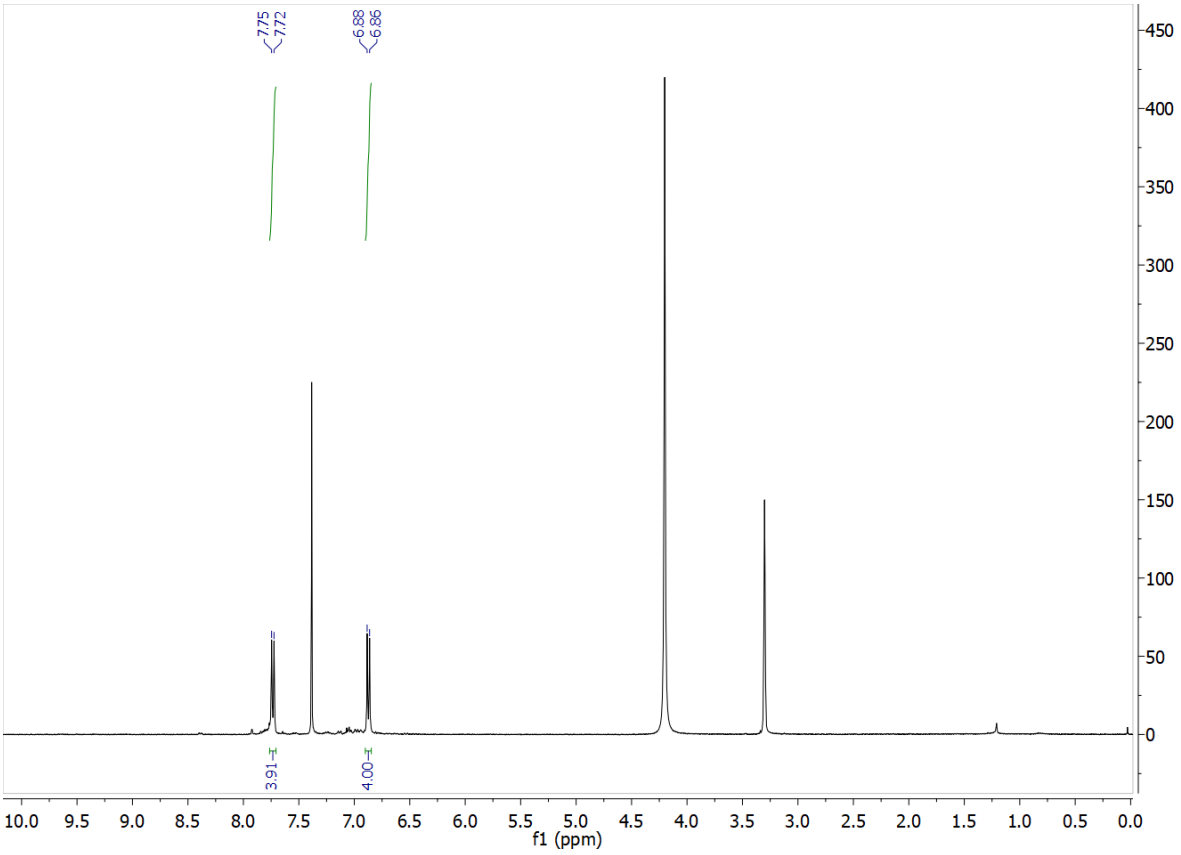

Compound 10 (^{1}H NMR, 400 MHz, $CDCl_3$)

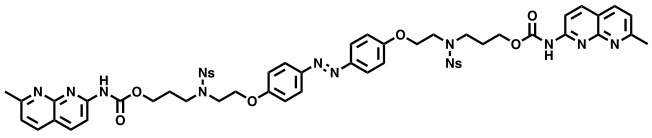

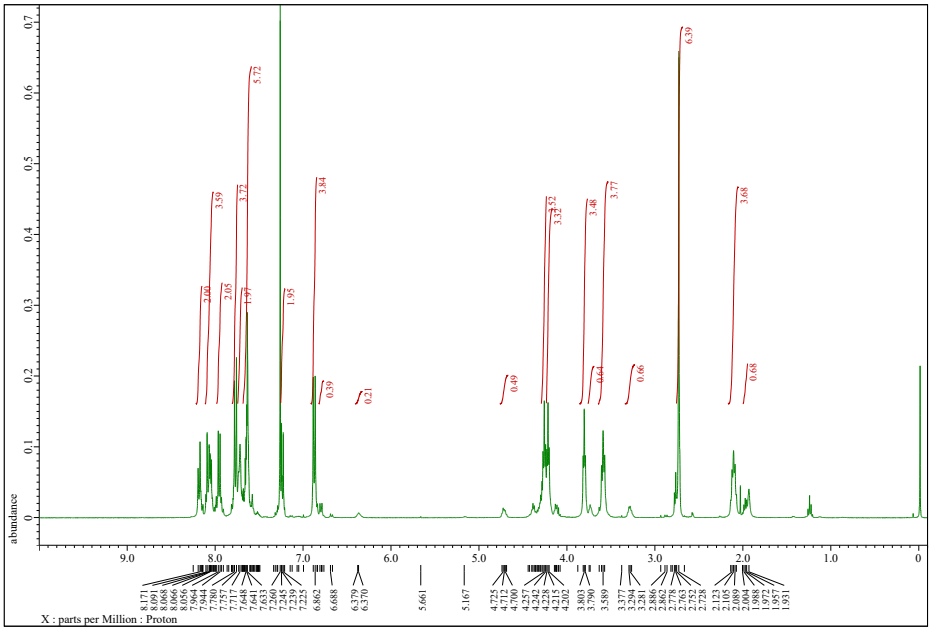

Compound 10 (^{13}C NMR, 100 MHz, $CDCl_3$)

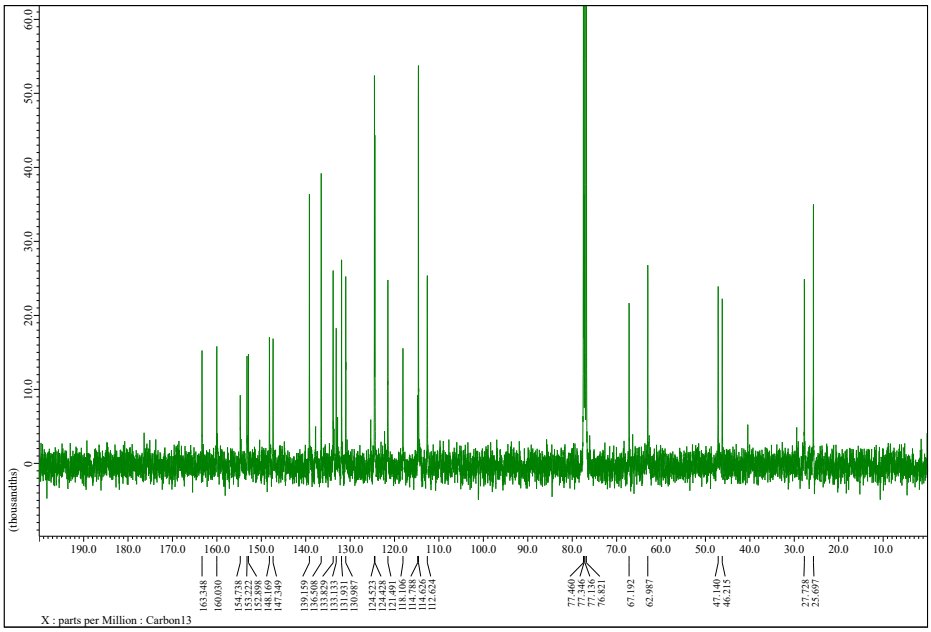

Compound 2 (^{1}H NMR, 700 MHz, CD_3OD)

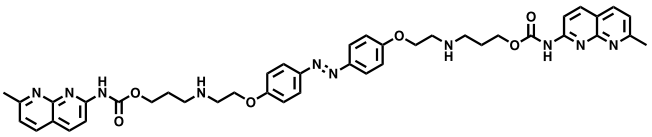

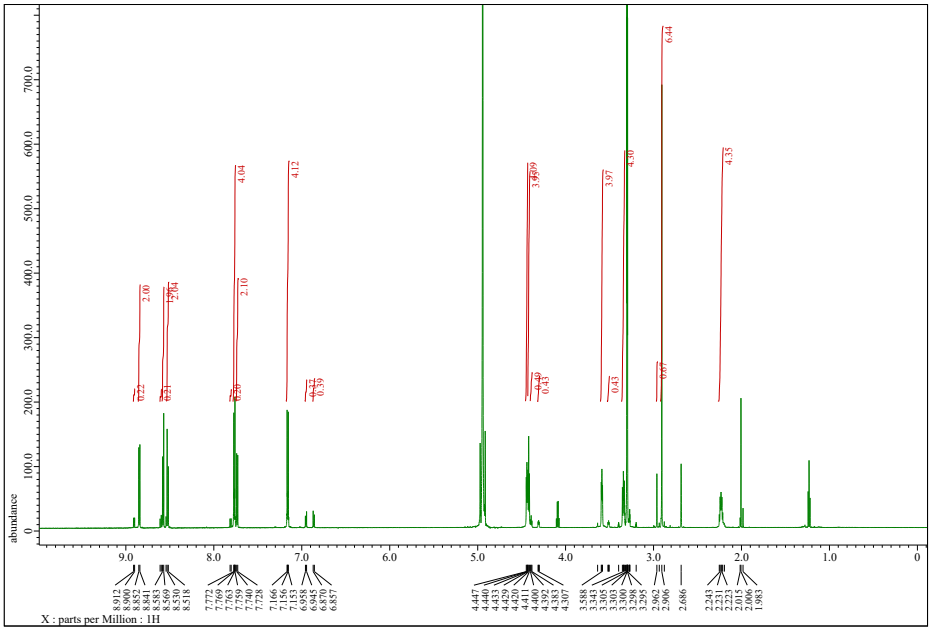

Compound 2 (^{13}C NMR, CD_3OD, 176 MHz)

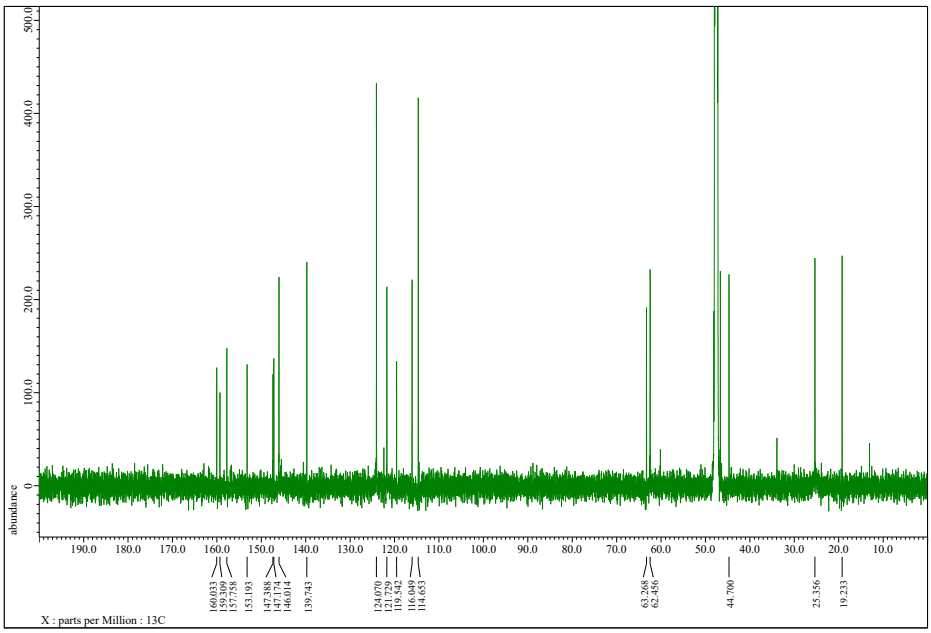

Compound 11 (^{1}H NMR, 400 MHz, $CDCl_3$)

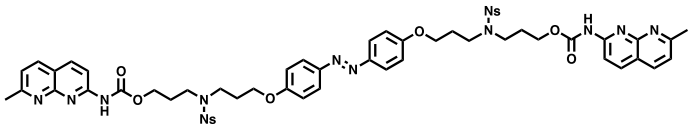

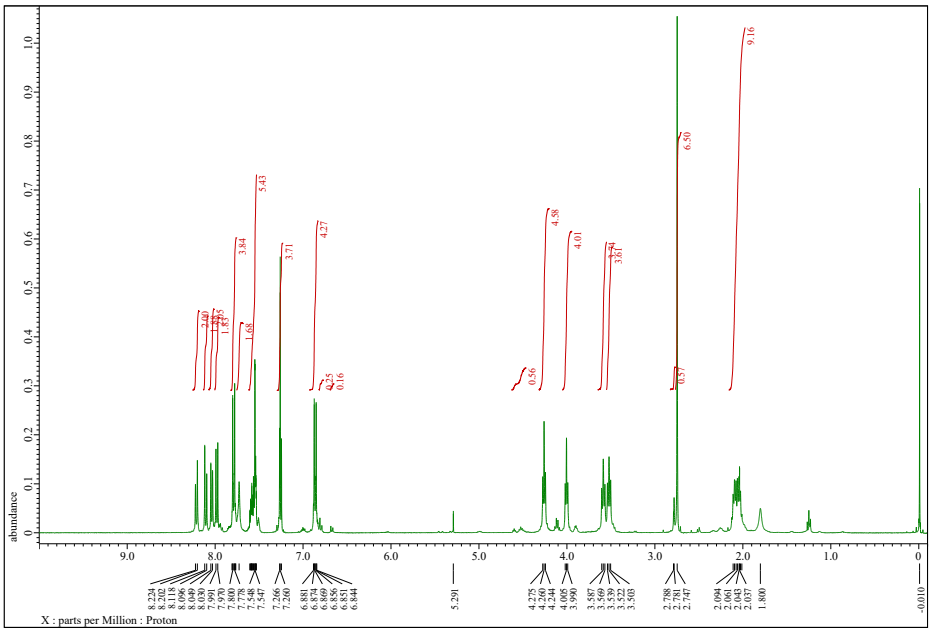

Compound 11 (^{13}C NMR, 100 MHz, $CDCl_3$)

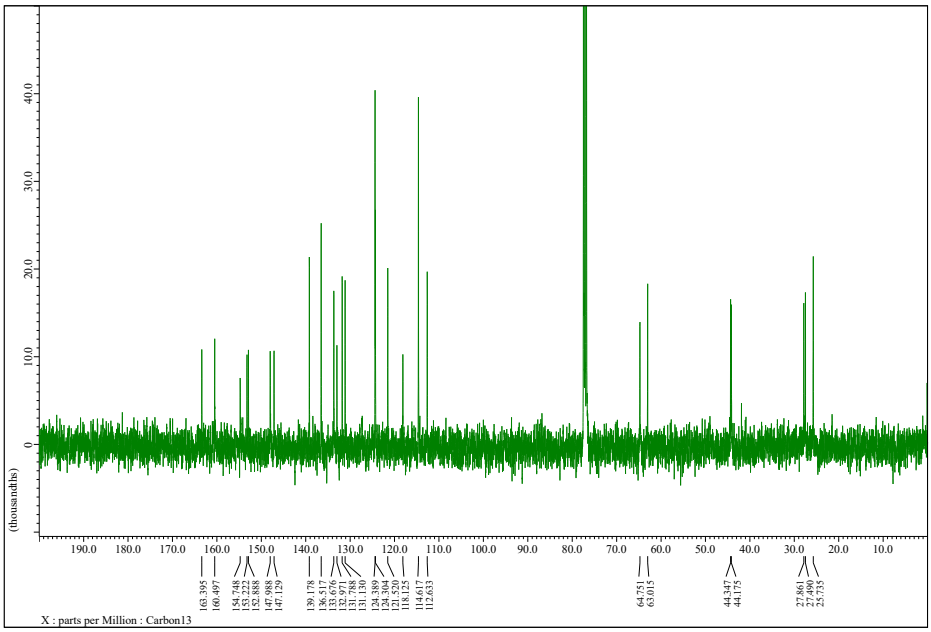

Compound 3 (^{1}H NMR, 700 MHz, CD_3OD)

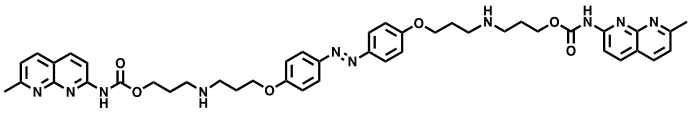

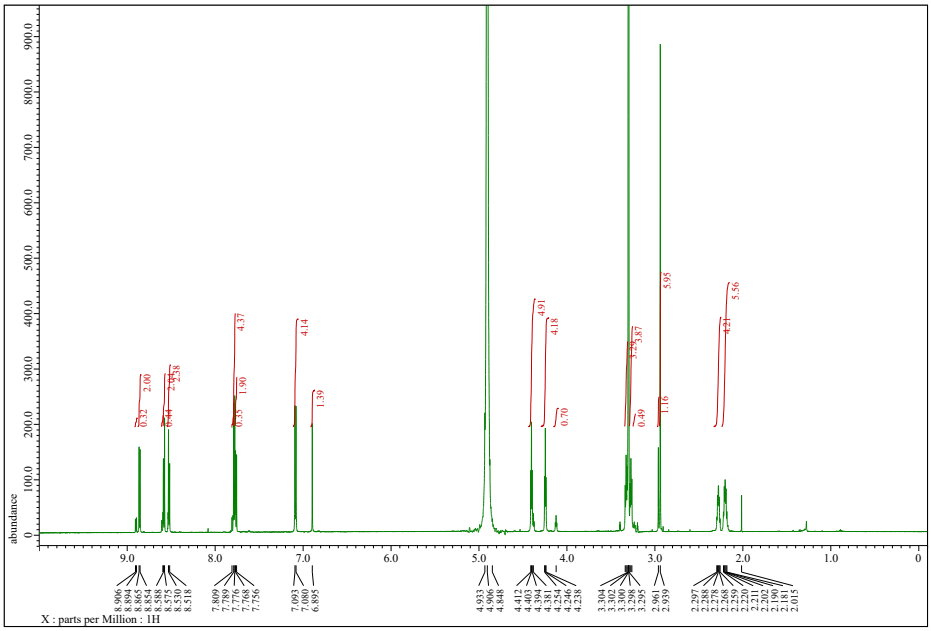

Compound 3 (^{13}C NMR, CD_3OD, 176 MHz)

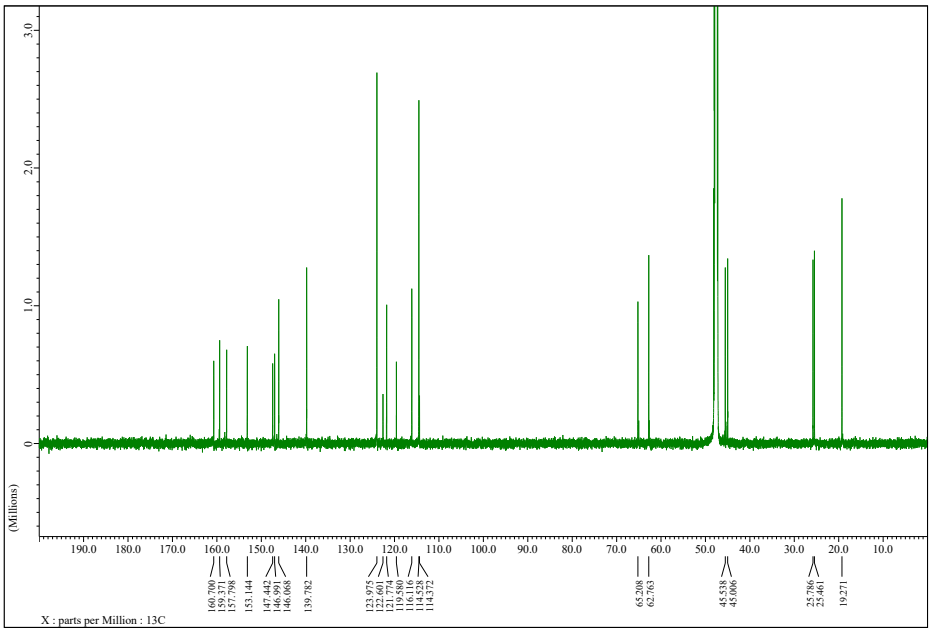

Compound 13 (^{1}H NMR; 400 MHz, Acetone-d_6)

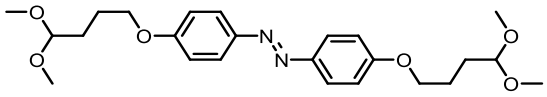

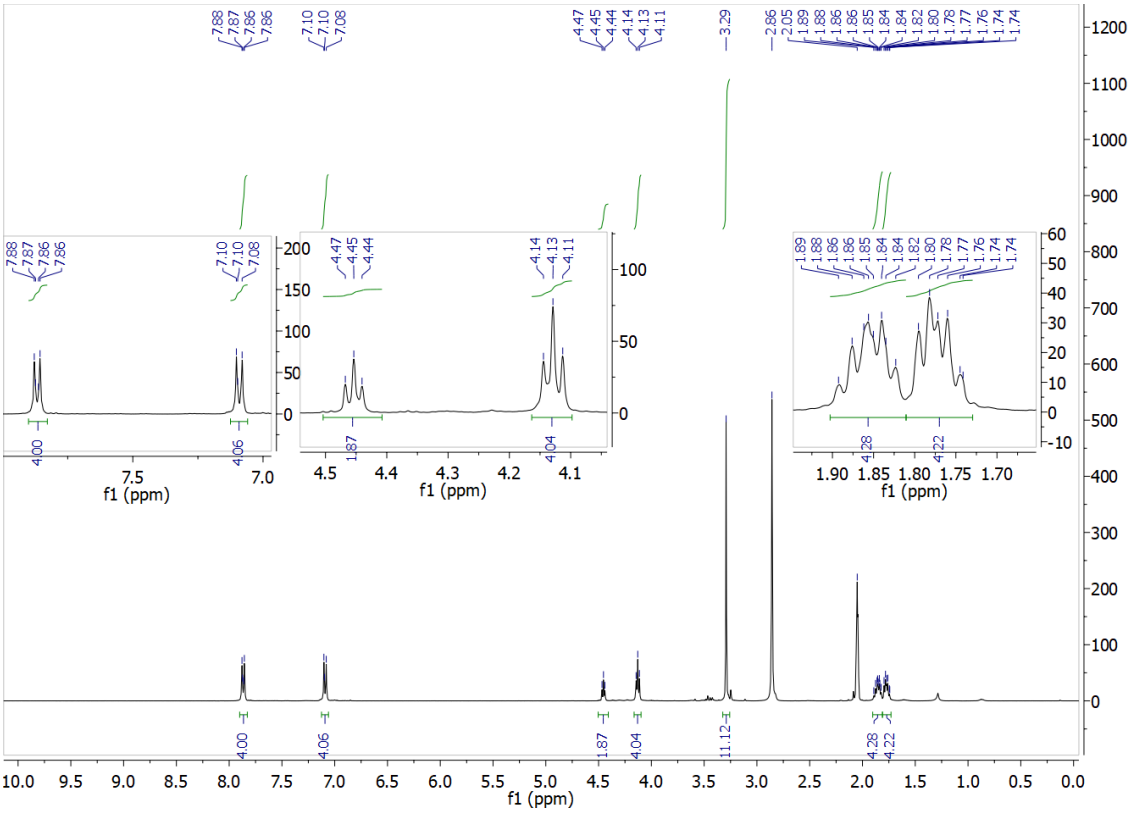

Compound 13 (^{13}C NMR; 101 MHz, Acetone-d_6)

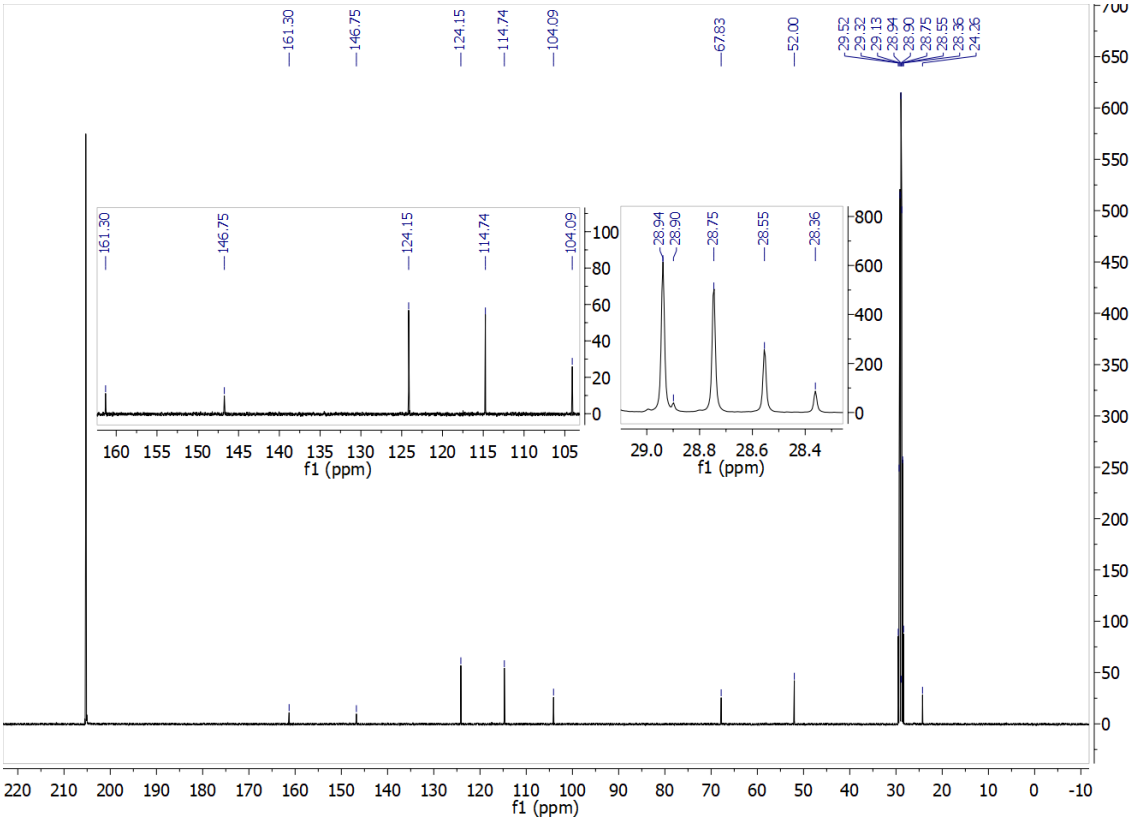

Compound 14 (^{1}H NMR, 400 MHz, Acetone-d_6)

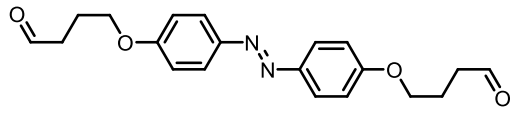

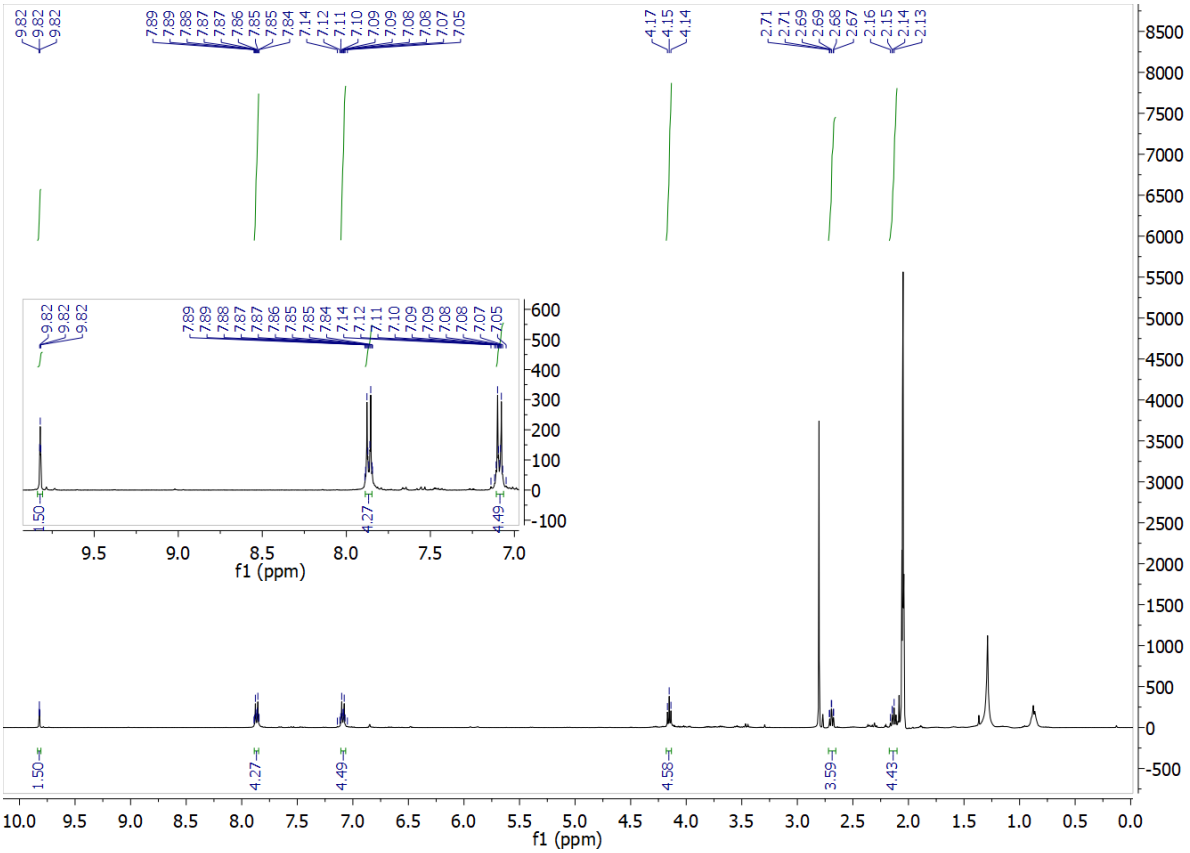

Compound 4 (^{1}H NMR, 700 MHz, CD_3OD)

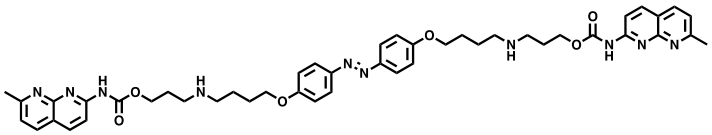

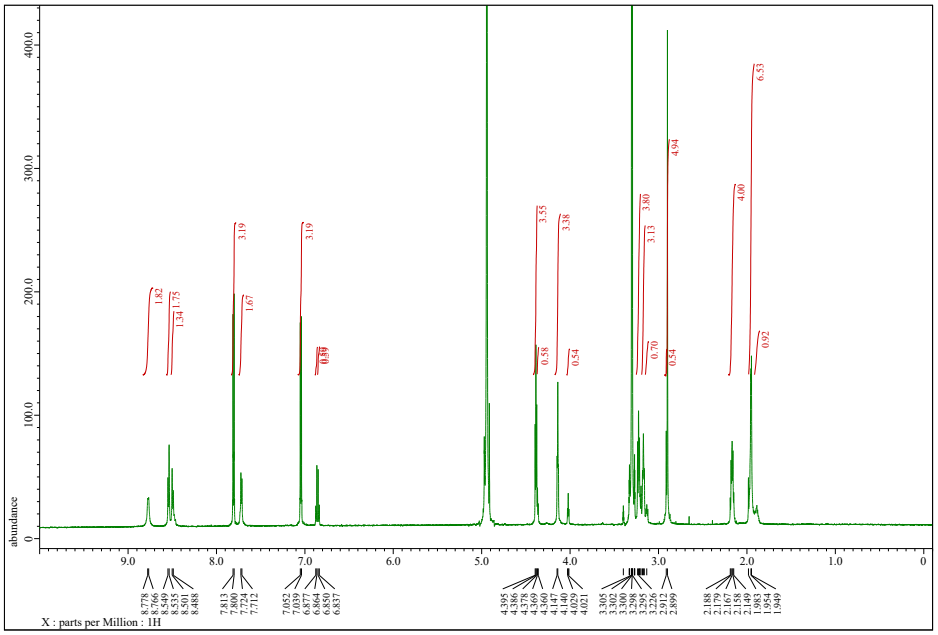

Compound 4 (^{13}C NMR, CD_3OD, 176 MHz)

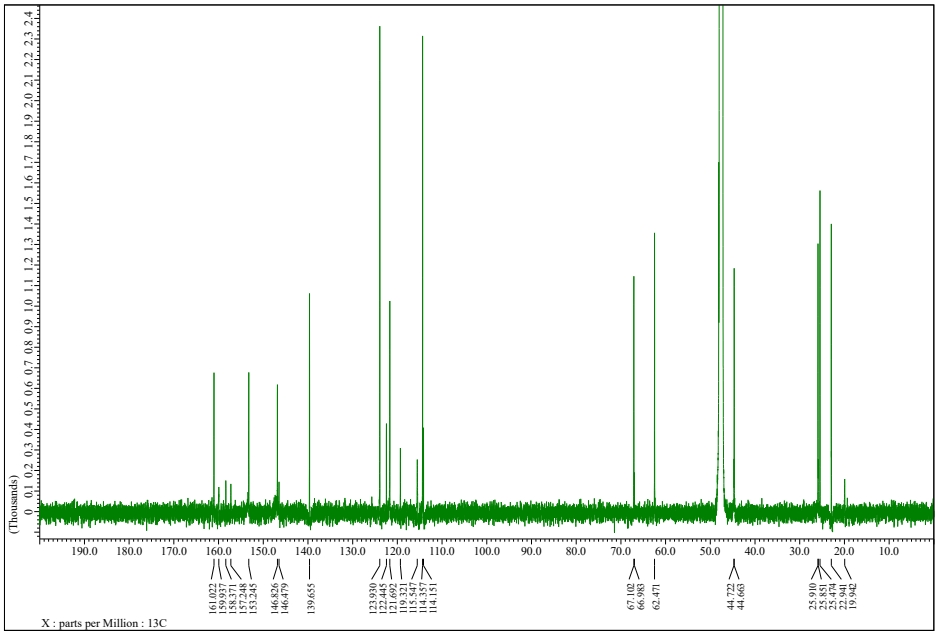

8. References

1 O. K. Rasheed, J. Raftery and P. Quayle, A New Benzannulation Reaction of Azoaromatics, *Synlett*, 2015, **26**, 2806–2810.

2 C. Dohno, T. Yamamoto and K. Nakatani, Photoswitchable unsymmetrical ligand for DNA hetero-mismatches, *Eur. J. Org. Chem.*, 2009, 4051–4058.

3 D. Koley, K. Srinivas, Y. Krishna and A. Gupta, A biomimetic approach for bicyclic alkaloids using acetal pro-nucleophile: total synthesis of (±)-epilupinine and formal syntheses of (±)-laburnine, (±)-isoretronecanol, (±)-tashiromine, *RSC Adv.*, 2014, **4**, 3934–3937.

4 C. Dohno, S. Uno and K. Nakatani, Photoswitchable Molecular Glue for DNA, *J. Am. Chem. Soc.*, 2007, **129**, 11898–11899.

5 K. Stranius and K. Börjesson, Determining the Photoisomerization Quantum Yield of Photoswitchable Molecules in Solution and in the Solid State, *Sci. Rep.*, 2017, **7**, 41145.

6 J. G. Calvert and J. N. Pitts, *Photochemistry*, John Wiley & Sons, Inc., New York - London - Sydney, 1st edn., 1966.

7 E. Freire, O. L. Mayorga and M. Straume, Isothermal titration calorimetry, *Anal. Chem.*, 1990, **62**, 950A-959A.

8 M. J. Frisch, G. W. Trucks, H. B. Schlegel, G. E. Scuseria, M. A. Robb, J. R. Cheeseman, G. Scalmani, V. Barone, G. A. Petersson, H. Nakatsuji, X. Li, M. Caricato, A. V. Marenich, J. Bloino, B. G. Janesko, R. Gomperts, B. Mennucci, H. P. Hratchian, J. V. Ortiz, A. F. Izmaylov, J. L. Sonnenberg, D. Williams-Young, F. Ding, F. Lipparini, F.; Egidi, J. Goings, B. Peng, A. Petrone, T. Henderson, D. Ranasinghe, V. G. Zakrzewski, J. Gao, N. Rega, G. Zheng, W. Liang, M. Hada, M. Ehara, K. Toyota, R. Fukuda, J. Hasegawa, M. Ishida, T. Nakajima, Y. Honda, O. Kitao, H. Nakai, T. Vreven, K. Throssell, J. A. J. Montgomery, J. E. Peralta, F. Ogliaro, M. J. Bearpark, J. J. Heyd, E. N. Brothers, K. N. Kudin, V. N. Staroverov, T. A. Keith, R. Kobayashi, J. Normand, K. Raghavachari, A. P. Rendell, J. C. Burant, S. S. Iyengar, J. Tomasi, M. Cossi, J. M. Millam, M. Klene, C. Adamo, R. Cammi, J. W. Ochterski, R. L. Martin, K. Morokuma, O. Farkas, J. B. Foresman and D. J. Fox, 2016, Gaussian 16, Revision C.01.

9 M. Cossi, N. Rega, G. Scalmani and V. Barone, Energies, structures, and electronic properties of molecules in solution with the C-PCM solvation model, *J. Comput. Chem.*, 2003, **24**, 669–681.

10 K. Roos, C. Wu, W. Damm, M. Reboul, J. M. Stevenson, C. Lu, M. K. Dahlgren, S. Mondal, W. Chen, L. Wang, R. Abel, R. A. Friesner and E. D. Harder, OPLS3e: Extending Force Field Coverage for Drug-Like Small Molecules, *J. Chem. Theory Comput.*, 2019, **15**, 1863–1874.

11 M. J. Abraham, T. Murtola, R. Schulz, S. Páll, J. C. Smith, B. Hess and E. Lindahl, GROMACS: High performance molecular simulations through multi-level parallelism from laptops to supercomputers, *SoftwareX*, 2015, **1**–**2**, 19–25.

12 K. Nakatani, S. Hagihara, Y. Goto, A. Kobori, M. Hagihara, G. Hayashi, M. Kyo, M. Nomura, M. Mishima and C. Kojima, Small-Molecule Ligand Induces Nucleotide Flipping in (Cag)n Trinucleotide Repeats, *Nat. Chem. Biol.*, 2005, **1**, 39–43.

13 J. Wang, W. Wang, P. A. Kollman and D. A. Case, Automatic atom type and bond type perception in molecular mechanical calculations, *J. Mol. Graph. Model.*, 2006, **25**, 247–260.

14 X. Zheng, D. Wang, Z. Shuai and X. Zhang, Molecular Dynamics Simulations of the Supramolecular Assembly between an Azobenzene-Containing Surfactant and α-Cyclodextrin: Role of Photoisomerization, *J. Phys. Chem. B*, 2012, **116**, 823–832.

15 U. Essmann, L. Perera, M. L. Berkowitz, T. Darden, H. Lee and L. G. Pedersen, A smooth particle mesh Ewald method, *J. Chem. Phys.*, 1995, **103**, 8577–8593.

16 S. Spicher and S. Grimme, Robust Atomistic Modeling of Materials, Organometallic, and Biochemical Systems, *Angew. Chem. Int. Ed.*, 2020, **59**, 15665–15673.